

# A linear second order IMEX all Mach scheme for the compressible Navier-Stokes system

Paola Allegrini<sup>1</sup> and Marie-Hélène Vignal<sup>1\*</sup>

<sup>1</sup>Institut de Mathématiques de Toulouse, Université de Toulouse, 118 route de Narbonne, Toulouse, 31062, France.

\*Corresponding author(s). E-mail(s): [mhvignal@math.univ-toulouse.fr](mailto:mhvignal@math.univ-toulouse.fr);  
Contributing authors: [pallegrini75@gmail.com](mailto:pallegrini75@gmail.com);

## Abstract

We propose and study an Implicit-Explicit (IMEX) finite volume scheme for the compressible Navier-Stokes system which is asymptotically preserving in the low-Mach number limit. The scheme is based on a flux splitting for the convective terms, allowing for the separation of slow terms propagating at the fluid velocity from fast terms propagating at the pressure wave velocity. The slow convective terms are then discretized explicitly, and the fast terms are discretized implicitly like the diffusive terms in order to avoid the quadratic constraint on the time step in viscous regimes. Then, we show how to linearize the pressure equation in order to obtain a linear and decoupled scheme: each conservative variable is solved separately. We prove the asymptotic consistency of the time semi-discretization and also show how to add spatial upwinding to the part of the convective flux treated implicitly in order to approach an  $L^\infty$  stability and thus eliminate non-physical oscillations commonly encountered when a scheme is only  $L^2$  stable. This scheme is extended to second order accuracy in time and space and validated by numerical tests in two dimensions with different types of fluids and compressible regimes.

**Keywords:** Asymptotic Preserving schemes, IMEX schemes, Low Mach number limit, Second-order schemes, Navier-Stokes system.

## Contents

<b>1</b>	<b>Introduction</b>	<b>2</b>
1.1	Scaling of the Navier-Stokes equations and review . . . . .	3

1.2	The formal low Mach number limit of the Navier Stokes equations . . .	5
<b>2</b>	<b>The first-order AP scheme</b>	<b>6</b>
2.1	The semi-discretization in time . . . . .	6
2.2	Asymptotic consistency . . . . .	8
2.3	Full discretization in one dimension, the first order $L^2$ -AP-scheme . . .	10
2.4	The first order implicit upwinding . . . . .	12
2.5	Asymptotic stability : C.F.L. condition on the time step . . . . .	14
<b>3</b>	<b>The second order AP-schemes</b>	<b>14</b>
<b>4</b>	<b>Numerical simulations</b>	<b>18</b>
4.1	2D Riemann problem . . . . .	18
4.2	Explosion problem . . . . .	20
4.3	First problem of Stokes . . . . .	21
4.4	Double shear layer: Incompressible solution . . . . .	22
4.5	Heat conduction . . . . .	23
4.6	Lid-driven cavity flow: steady state incompressible solution . . . . .	24
<b>5</b>	<b>Conclusion</b>	<b>25</b>

## 1 Introduction

The study and numerical simulation of certain fluid flows require the consideration of regime transitions such as the transitions from the compressible regime to the incompressible regime, see for example the study of lightning strikes on airlines [1], [2]. These transitions between the compressible and incompressible regimes are well understood from a continuous point of view, whether for the Euler [3–6] or Navier-Stokes equations [7–10]. They are linked to the variations in time and/or space of the Mach number, which is the ratio between the speed of the fluid and that of the pressure waves in the fluid. When the Mach number is small, the pressure waves propagate at very high speeds and the incompressible regime is reached. The compressible Euler or Navier-Stokes models then tend towards their incompressible version in the limit of the Mach number tending towards 0.

From a numerical simulation perspective, the only models capable of describing all regimes are the compressible models. And, if the schemes used to discretise these models are not designed to handle transitions towards incompressibility, the meshes will have to follow the rapid pressure waves. As a result, very small time steps are required to ensure the stability of the schemes. Furthermore, even when the schemes are stable, it may sometimes be necessary to modify them to achieve the asymptotic consistency of the scheme, meaning the ability to capture the incompressible solution as the Mach number tends to 0.

Finally, these transitions can occur in time but also in space. Then, at a given time, the fluid may be in the compressible regime in one part of the domain, in the incompressible regime in another part, and in a transient regime in the remainder of the domain. Therefore, even if the incompressible region is small, it imposes the use

of small time steps, including in the compressible regions, which can make simulations very costly.

## 1.1 Scaling of the Navier-Stokes equations and review

Let us first present the model and the low Mach regime rescaling that we consider in this paper. We denote by  $t > 0$  the time and by  $x \in \Omega$  the space variable where  $\Omega \subset \mathbb{R}^d$  ( $d = 1, 2$  or  $3$ ) is an open bounded domain. We consider a fluid described by its density  $\rho(t, x) \geq 0$ , its velocity  $U(t, x) \in \mathbb{R}^d$  and its total energy  $E(t, x)$  satisfying the compressible Navier-Stokes equations:

$$\partial_t \rho + \nabla \cdot (\rho U) = 0, \quad (1a)$$

$$\partial_t (\rho U) + \nabla \cdot \left( \frac{\rho U \otimes U}{\rho} \right) + \nabla p = \nabla \cdot \sigma, \quad (1b)$$

$$\partial_t E + \nabla \cdot ((E + p)U) = \nabla \cdot (\sigma U) + \nabla \cdot (\lambda \nabla T), \quad (1c)$$

where  $p$  is the pressure given by an equation of state, here that of perfect gases:

$$E = \frac{p}{\gamma - 1} + \frac{\rho |U|^2}{2}, \quad (1d)$$

with  $\gamma = c_p/c_v > 1$  the ratio of specific heats. The viscous stress tensor is given by

$$\sigma = \mu (\nabla U + (\nabla U)^T) - \frac{2}{3} \mu (\nabla \cdot U) \text{Id}_{\mathbb{R}^d}, \quad (1e)$$

with  $\text{Id}_{\mathbb{R}^d} \in \mathbb{R}^{d \times d}$  the identity matrix and  $\mu$  the given dynamical viscosity coefficient. Finally,  $\lambda$  is the given thermal conductivity coefficient and  $T$  the fluid temperature which for a perfect gas is given by the relation

$$p = R\rho T, \quad (1f)$$

with  $R = c_p - c_v$  the specific gas constant.

The characteristic Mach number in the fluid is given by  $M_0 = u_0/c_0$  where  $u_0$  and  $c_0$  are respectively the characteristic fluid velocity norm and pressure waves velocity norm. More precisely  $c_0 = \sqrt{\gamma p_0/\rho_0}$  where  $p_0$  and  $\rho_0$  are the characteristic pressure and density in the fluid. Using these characteristic quantities as well as the characteristic length  $x_0$  and time  $t_0 = x_0/u_0$ , we rescale the previous system of equations. We define the rescaled variables  $\tilde{x} = x/x_0$ ,  $\tilde{t} = t/t_0$  and introduce the rescaled quantities  $\tilde{\rho}(\tilde{t}, \tilde{x}) = \rho(t, x)/\rho_0$ ,  $\tilde{U}(\tilde{t}, \tilde{x}) = U(t, x)/u_0$ ,  $\tilde{p}(\tilde{t}, \tilde{x}) = p(t, x)/p_0$ ,  $\tilde{E}(\tilde{t}, \tilde{x}) = E(t, x)/p_0$ ,  $\tilde{\mu} = \mu/(\rho_0 u_0 x_0)$ ,  $\tilde{\lambda} = \lambda/(\rho_0 u_0 x_0)$  and  $\tilde{T}(\tilde{t}, \tilde{x}) = T(t, x)/T_0$  where  $T_0 = p_0/\rho_0$ . Omitting the ‘‘tildes’’, we obtain

$$\partial_t \rho + \nabla \cdot (\rho U) = 0, \quad (2a)$$

$$\partial_t (\rho U) + \nabla \cdot \left( \frac{\rho U \otimes U}{\rho} \right) + \frac{1}{\varepsilon} \nabla p = \nabla \cdot \sigma, \quad (2b)$$

$$\partial_t E + \nabla \cdot ((E + p)U) = \varepsilon \nabla \cdot (\sigma U) + \nabla \cdot (\lambda \nabla T), \quad (2c)$$

$$E = \frac{p}{\gamma - 1} + \frac{\rho |U|^2}{2\varepsilon}, \quad (2d)$$

where the rescaled parameter  $\varepsilon$  is of the order of the square of the Mach-number, more precisely  $\varepsilon = \gamma M_0^2$  and where the rescaled viscous stress tensor and temperature are still given by (1e) and (1f).

The previous system can be rewritten in a compact form as

$$\partial_t W + \nabla \cdot F(W) = \nabla \cdot (G(W, \nabla W)), \quad (3)$$

where  $W = (\rho, \rho U, E)$  is the vector of conserved variables,  $F(W) = (\rho U, \rho U \otimes U + 1/\varepsilon p \text{Id}_{\mathbb{R}^d}, (E + p)U)$  is the inviscid flux for the Euler equations and  $G(W, \nabla W) = (0, \sigma, \varepsilon \sigma \cdot U + \lambda \nabla T)$  is the diffusion flux.

In Low-Mach regimes, the typical sound speed in the fluid,  $c_0$ , is very large compared to the typical speed of the fluid itself,  $U_0$ , and so  $\varepsilon$  is very small. In such situations, if an explicit scheme is used, the time step must satisfy a severe CFL (Courant-Friedrichs-Levy) stability condition otherwise it is unstable (see [11] for instance). Indeed, if  $d = 2$ , even if the diffusive terms,  $G$ , are treated implicitly, the CFL condition, ensuring the stability of solvers explicit on the convective part,  $F$ , for the time step  $\Delta t$  is given by

$$\Delta t \leq \frac{C}{\frac{\max(|u \pm c/\sqrt{\varepsilon}|)}{\Delta x} + \frac{\max(|v \pm c/\sqrt{\varepsilon}|)}{\Delta y}},$$

where  $C$  is a constant depending on the chosen scheme,  $\Delta x$  and  $\Delta y$  are the space steps and  $U = (u, v)$ . Then, for given space steps  $\Delta x$  and  $\Delta y$ , the time step  $\Delta t$  is of order  $\sqrt{\varepsilon}$  and tends to 0 with  $\varepsilon$ . Furthermore, even if this constraint is satisfied, it is well known (see [12], [13] or [14]) that explicit schemes suffer from a consistency problem in the limit  $\varepsilon \rightarrow 0$ . Indeed, they are not capable to capture the right asymptotic regime. Solutions have been proposed to bypass this asymptotic consistency problem (see [14], [15], [16]), but, the stability constraint on the time step still remains. A possible way to bypass these limitations is to use an asymptotic preserving scheme which is consistent with the limit and free of the constraints related to the Mach number  $\varepsilon$ . In practice, asymptotic preserving schemes can be obtained using IMEX methods [17, 18].

Here, we split the flux  $F$  into two parts  $F = F_e + F_i$ . The first part  $F_e$  will be treated explicitly while the second one,  $F_i$ , implicitly. The choice of the flux splitting must be well chosen in order to obtain asymptotic stability, asymptotic consistency and with a reasonable computational cost. In [19] we defined, for the full Euler equations, criteria in order to choose correctly the right flux decomposition respecting the above properties. In this article we propose to use the same decomposition of  $F$ , the one introduced by E.F. Toro, M.E. Vázquez-Cendón in [20] for ensuring the recognition of contact discontinuities and shear waves. Moreover, in the case of strongly viscous flows, if the viscous terms,  $G$  are explicitly treated, the time step must obey a quadratic

restriction proportional to  $\Delta x^2 / \max(\mu, \lambda)$ , and this condition on the maximum time step can become rather severe for large values of  $\mu$  or  $\lambda$ . To also overcome those restrictions, we propose to treat implicitly the diffusion flux,  $G$ . Since it contains only linear terms, we consider that this choice of treatment adds a reasonable computational cost and allows us to use larger time steps in strongly viscous regimes as well.

First, we recall in the next section the formal low-Mach number limit. We present our first order asymptotic preserving discretization in section 2 and we prove its asymptotic consistency in the low-Mach number limit. We propose both a centered approximation for the implicit part of the flux, which is only  $L^2$  stable and an upwind approximation that allows for a closer approach to a more robust  $L^\infty$  stability. We extend our scheme to second order accuracy in section 3. Then, we show the good behavior of our second-order AP scheme through several two-dimensional test-cases involving non-viscous fluids, viscous fluids, and fluids with heat conduction. These numerical results show that our scheme allows the simulation of fluid flows in regimes ranging from compressible to incompressible, that is, for Mach number values ranging from order 1 to 0.

## 1.2 The formal low Mach number limit of the Navier Stokes equations

The rigorous low Mach number limit of the isentropic Navier-Stokes equations has been well investigated in the last years [8–10] for the isentropic case and [7, 21] for the non-isentropic case. Here, we briefly recall the formal limit. We denote by  $(\rho_\varepsilon, q_\varepsilon, E_\varepsilon, p_\varepsilon, T_\varepsilon)$  the solution of (2) with the boundary conditions  $U_\varepsilon \cdot \nu = 0$  and  $\nabla T_\varepsilon \cdot \nu n = 0$  on  $\partial\Omega$  where  $\nu$  is the unit normal to  $\partial\Omega$  outward to  $\Omega$ .

Passing to the limit into the momentum equation of system (2), we obtain that  $\nabla p_0(x, t) = 0$  and so  $p_0(x, t) = p^0(t)$  for all  $x \in \Omega$  and  $t > 0$ . The limit of the equation of state (2d) gives  $E_0(x, t) = E_0(t) = p_0(t)/(\gamma - 1)$  for all  $x \in \Omega$  and  $t > 0$ . Passing to the limit in the energy equation the viscous term disappears. Then, integrating on  $\Omega$  we obtain using the boundary conditions for all  $t > 0$ ,

$$|\Omega| E_0'(t) + (E_0(t) + p_0(t)) \int_{\partial\Omega} U_0 \cdot n(x) d\sigma(x) - \lambda \int_{\partial\Omega} \nabla T_0 \cdot \nu d\tau(x) = |\Omega| E_0'(t) = 0.$$

Then,  $E_0(t) = E_0 = 1/|\Omega| \int_{\Omega} E_0(x, 0) dx = \langle E_0(\cdot, 0) \rangle$  since the initial condition can be not well prepared to the low-Mach number limit. Finally, assuming that  $p_1(x, t) = \lim_{\varepsilon \rightarrow 0} \frac{1}{\varepsilon} (p_\varepsilon(x, t) - p_0)$  exists, we recover the Low Mach limit system

$$\partial_t \rho_0 + \nabla \cdot (\rho_0 U_0) = 0, \tag{4a}$$

$$\partial_t (\rho_0 U_0) + \nabla \cdot \left( \frac{\rho_0 U_0 \otimes U_0}{\rho_0} \right) + \nabla p_1 = \nabla \cdot \sigma_0, \tag{4b}$$

$$\gamma \nabla \cdot U_0 = (\gamma - 1) \nabla \cdot \left( \frac{\lambda}{R} \nabla \left( \frac{1}{\rho_0} \right) \right), \tag{4c}$$

$$E_0 = \frac{p_0}{\gamma - 1} = \frac{1}{|\Omega|} \int_{\Omega} E_0(x, 0) dx. \tag{4d}$$

Let us remark that we do not have the incompressibility constraint  $\nabla \cdot U_0 = 0$ , this is due to the combined effects of large temperature variations and thermal conduction. Neglecting the heat conduction effects i.e setting  $\lambda = 0$  we recover the Navier-Stokes incompressible model. Moreover neglecting also the viscous forces, i.e. setting  $\mu$  to zero, we obtain the low Mach limit for the compressible Euler equations.

## 2 The first-order AP scheme

### 2.1 The semi-discretization in time

As explained in the introduction, we use an IMEX scheme which consists of splitting the transport flux terms into a slow convective part related to the fluid velocity and a fast convective part related to the pressure wave velocity. The slow convective part is then treated explicitly and the fast convective part, as well as the diffusive terms, are treated implicitly. This flux-splitting is more complex in the present case than in the isentropic case for which it is well identified and widely used in the literature [22], [23], [24], [25], [26], [27]. For the system considered here, we rely on the study carried out in [19] on several flux splittings proposed in the literature for the Euler system and use the one initially introduced in [20] for building schemes which ensure the recognition of contact discontinuities and shear waves and then used in [28], [29], [19], [30] to construct AP schemes in the low-Mach limit for the full Euler or Navier-Stokes system.

For a uniform discretization in time (for clarity) where  $\Delta t$  denotes the time step, we first consider the following first order semi-discretization:

$$\frac{W^{n+1} - W^n}{\Delta t} + \nabla \cdot F_e(W^n) + \nabla \cdot F_i(W^{n+1}) = \nabla \cdot G(W^{n+1}, \nabla W^{n+1}), \quad (5a)$$

$$E^{n+1} = \frac{p^{n+1}}{\gamma - 1} + k^{n+1}. \quad (5b)$$

where the explicit and implicit inviscid fluxes are given by  $F_e(W) = (\rho U, \rho U \otimes U, k_\varepsilon U)$  and  $F_i(W) = (0, p/\varepsilon, hU)$  with  $k_\varepsilon = k_\varepsilon(W) = \varepsilon \rho |U|^2/2$  the kinetic energy and  $h = h(W) = \gamma(E - k_\varepsilon)$  the specific enthalpy and the implicit diffusion flux is given by  $G_i(W, \nabla W) = (0, \sigma, \varepsilon \sigma \cdot U + \lambda \nabla T)$ .

Inserting the momentum equation into the inviscid flux for the energy equation and expressing  $E^{n+1}$  with the equation of state and multiplying by  $\varepsilon$ , one recovers the discretization of the pressure wave equation into the fluid which yields an elliptic equation for determining the unknown pressure  $p^{n+1}$ :

$$\begin{aligned} \frac{\varepsilon}{\gamma - 1} p^{n+1} - \Delta t^2 \nabla \cdot \left( \frac{h^{n+1}}{\rho^{n+1}} \nabla p^{n+1} \right) - \frac{\varepsilon \Delta t \lambda}{R} \Delta \left( \frac{p^{n+1}}{\rho^{n+1}} \right) &= -\varepsilon k^{n+1} + \varepsilon E^{n+1, exp} \\ -\varepsilon \Delta t \nabla \cdot \left( \frac{h^{n+1}}{\rho^{n+1}} ((\rho U)^{n+1, exp} + \Delta t \nabla \cdot \sigma^{n+1}) \right) &+ \varepsilon^2 \Delta t \nabla \cdot \left( \sigma^{n+1} \frac{q^{n+1}}{\rho^{n+1}} \right), \end{aligned} \quad (6)$$

where the explicit convected part of the conservative variables  $W^{n+1,exp}$  is given by:

$$W^{n+1,exp} = \begin{pmatrix} \rho^{n+1,exp} \\ (\rho U)^{n+1,exp} \\ E^{n+1,exp} \end{pmatrix} = W^n - \Delta t \nabla \cdot F_e(W^n). \quad (7)$$

The equation on the unknown pressure is highly nonlinear, in [29, 30] the schemes consist in advancing the density for which the implicit part is zero, and calculating the momentum and pressure using (6) and the momentum equation with the use of a Picard algorithm. In practice, the convergence of this fixed point algorithm is not always guaranteed during simulations, and furthermore, it may lead to the resolution of non-symmetric linear systems. This is why, in our case, we prefer use a linear uncoupled scheme for  $p^{n+1}$  and  $q^{n+1}$  and avoid the Picard algorithm for reducing the computational cost. Following the same strategy as in [19], for the full Euler equations, the quantities  $h^{n+1}$  and  $k_\varepsilon^{n+1}$  are approximated by their explicit convected values  $k_\varepsilon^{n+1,exp} = k_\varepsilon(W^{n+1,exp})$  and  $h^{n+1,exp} = h(W^{n+1,exp})$ . Here we propose to also approximate the implicit viscous terms by their explicit convected values  $\sigma^{n+1,exp} = \sigma(W^{n+1,exp})$  and  $(\sigma U)^{n+1,exp} = (\sigma(W^{n+1,exp})U^{n+1,exp})$ . Doing so, we obtain a linear equation for the pressure  $p^{n+1}$ . After expressing the temperature with the state equation  $T = (\gamma - 1)(E - k_\varepsilon)/(R\rho)$  in the energy equation, our resulting semi-discretization is given by

$$\rho^{n+1} = \rho^n - \Delta t \nabla \cdot (\rho U)^n, \quad (8a)$$

$$\begin{aligned} \frac{\varepsilon}{\gamma - 1} p^{n+1} - \Delta t^2 \nabla \cdot \left( \frac{h^{n+1,exp}}{\rho^{n+1}} \nabla p^{n+1} \right) - \frac{\varepsilon \Delta t \lambda}{R} \Delta \left( \frac{p^{n+1}}{\rho^{n+1}} \right) = \varepsilon E^{n+1,exp} \\ - \varepsilon k_\varepsilon^{n+1,exp} - \varepsilon \Delta t \nabla \cdot \left( \frac{h^{n+1,exp}}{\rho^{n+1}} ((\rho U)^{n+1,exp} + \Delta t \nabla \cdot \sigma^{n+1,exp}) \right) \\ + \varepsilon^2 \Delta t \nabla \cdot (\sigma^{n+1,exp} U^{n+1,exp}) \end{aligned} \quad (8b)$$

$$(\rho U)^{n+1} - \Delta t \nabla \cdot \sigma^{n+1} = (\rho U)^{n+1,exp} - \frac{\Delta t}{\varepsilon} \nabla p^{n+1}, \quad (8c)$$

$$\begin{aligned} E^{n+1} = E^{n+1,exp} - \Delta t \nabla \cdot \left( \frac{\gamma p^{n+1}}{\gamma - 1} U^{n+1} \right) + \varepsilon \Delta t \nabla \cdot (\sigma^{n+1} U^{n+1}) \\ + \frac{\Delta t \lambda}{R} \Delta \left( \frac{p^{n+1}}{\rho^{n+1}} \right), \end{aligned} \quad (8d)$$

where

$$(\rho U)^{n+1,exp} = (\rho U)^n - \Delta t \nabla \cdot (\rho^n U^n \otimes U^n), \quad (8e)$$

$$E^{n+1,exp} = E^n - \Delta t \nabla \cdot (k_\varepsilon^n U^n), \quad (8f)$$

and where we recall that  $k_\varepsilon^{n+1,exp} = \varepsilon \rho^{n+1,exp} |U^{n+1,exp}|^2/2$  and  $h^{n+1,exp} = \gamma(E^{n+1,exp} - k_\varepsilon^{n+1,exp})$ .

The scheme consists in computing sequentially  $\rho^{n+1}$  with (8a),  $p^{n+1}$  with (8b),  $(\rho U)^{n+1}$  with (8c) and then  $E^{n+1}$  with (8d) where  $\sigma^{n+1}$  is known. Note that to compute  $q^{n+1}$  and  $E^{n+1}$  we need to solve a linear system since the viscous forces and

the heat flux are implicitly treated. This yields a condition on the time step  $\Delta t$  only related to the explicit convected flux  $F_e$ .

The resulting scheme is linear. We will see in numerical results that it is also asymptotically stable, the time step does not tend to 0 when  $\varepsilon$  tends to 0. Furthermore, in the next section we prove that it is also asymptotically consistent, i.e. we recover a semi-discretization of the compressible Navier-Stokes equations when  $\varepsilon$  tends to 0.

## 2.2 Asymptotic consistency

**Lemma 1** *Let  $\varepsilon, \Delta t > 0$  and we denote by  $(\rho^n, (\rho U)^n, E^n, p^n)_{n \geq 0}$  the solution to (8) with a given initial condition  $W^0 = (\rho^0, (\rho U)^0, E^0)$  and  $p^0 = E^0 - k_\varepsilon(W^0)$ . For all  $n \geq 0$ , we assume the boundary conditions given by  $U^n \cdot \nu = 0$  and  $\nabla T^n \cdot \nu = 0$  on  $\partial\Omega$  where  $\nu$  is the unit normal to  $\partial\Omega$  outward to  $\Omega$ . We assume that  $(\rho^n, (\rho U)^n, E^n, p^n)_{n \geq 0}$  converges toward  $(\rho_0^n, (\rho U)_0^n, E_0^n, p_0^n)_{n \geq 0}$  when  $\varepsilon \rightarrow 0$ . Then, for all  $n \geq 0$ , we have  $p_0^{n+1} = (\gamma - 1) \langle E_0^0 \rangle + \mathcal{O}(\Delta t^2)$  and  $E_0^{n+1} = \langle E_0^0 \rangle$  where  $E_0^0$  is the limit of the initial energy and  $\langle E_0^0 \rangle$  is its mean value on  $\Omega$ .*

*Furthermore, if the initial energy is well-prepared to the low-Mach number limit regime, more precisely if  $E_0(x, 0) = \lim_{\varepsilon \rightarrow 0} E_\varepsilon(x, 0) = \bar{E}_0 + \mathcal{O}(\Delta t^2)$  with  $\bar{E}_0$  constant, we recover the asymptotic consistency up to  $\mathcal{O}(\Delta t)$ , i.e. we have for all  $n \geq 0$   $\nabla p_0^{n+1} = 0$ ,  $E_0^{n+1} = \frac{p_0^{n+1}}{\gamma - 1} + \mathcal{O}(\Delta t^2) = \bar{E}_0 + \mathcal{O}(\Delta t^2)$  and  $\gamma \nabla \cdot U_0^{n+1} = (\gamma - 1) \frac{\lambda}{R} \Delta \left( \frac{1}{\rho_0^{n+1}} \right) + \mathcal{O}(\Delta t)$ .*

*Proof* We perform an asymptotic expansion for all quantities  $f^l = f_0^l + \varepsilon f_1^l$  with  $l = n, (n+1, exp)$  or  $n+1$ . Then, dividing (8b) by  $\varepsilon$  and inserting the asymptotic expansion of all quantities in System (8) yields:

$$\varepsilon^{-1} : \nabla \cdot \left( \frac{h_0^{n+1,exp}}{\rho_0^{n+1}} \nabla p_0^{n+1} \right) = 0$$

$$\nabla p_0^{n+1} = 0$$

$$\varepsilon^0 : \rho_0^{n+1} = \rho_0^n - \Delta t \nabla \cdot (\rho_0 U_0)^n,$$

$$(\rho_0 U_0)^{n+1,exp} = (\rho_0 U_0)^n - \Delta t \nabla \cdot (\rho_0^n U_0^n \otimes U_0^n),$$

$$E_0^{n+1,exp} = E_0^n,$$

$$\begin{aligned} \frac{p_0^{n+1}}{\gamma - 1} - \Delta t^2 \nabla \cdot \left( \frac{h_0^{n+1,exp}}{\rho_0^{n+1}} \nabla p_1^{n+1} + \left( \frac{h_0^{n+1,exp}}{\rho_0^{n+1}} \right)_1 \nabla p_0^{n+1} \right) - \frac{\Delta t \lambda}{R} \Delta \left( \frac{p_0^{n+1}}{\rho_0^{n+1}} \right) \\ = E_0^{n+1,exp} - \Delta t \nabla \cdot \left( \frac{h_0^{n+1,exp}}{\rho_0^{n+1}} \left( (\rho_0 U_0)^{n+1,exp} + \Delta t \nabla \cdot \sigma_0^{n+1,exp} \right) \right), \end{aligned}$$

$$(\rho_0 U_0)^{n+1} - \Delta t \nabla \cdot \sigma_0^{n+1} = (\rho_0 U_0)^{n+1,exp} - \Delta t \nabla p_1^{n+1},$$

$$E_0^{n+1} = E_0^{n+1,exp} - \Delta t \nabla \cdot \left( \frac{\gamma p_0^{n+1}}{\gamma - 1} U_0^{n+1} \right) + \frac{\Delta t \lambda}{R} \Delta \left( \frac{p_0^{n+1}}{\rho_0^{n+1}} \right).$$

Now, remarking that  $h_0^{n+1,exp} = \gamma E_0^{n+1,exp} = \gamma E_0^n$ , and inserting the momentum equation into the pressure equation, we obtain:

$$\begin{aligned} \varepsilon^{-1} : \nabla p_0^{n+1} &= 0 \\ \varepsilon^0 : \rho_0^{n+1} &= \rho_0^n - \Delta t \nabla \cdot (\rho_0 U_0)^n, \\ \frac{p_0^{n+1}}{\gamma - 1} - \frac{\Delta t \lambda p_0^{n+1}}{R} \Delta \left( \frac{1}{\rho_0^{n+1}} \right) &= E_0^n - \Delta t \nabla \cdot \left( \gamma E_0^n U_0^{n+1} + \Delta t \frac{\gamma E_0^n}{\rho_0^{n+1}} \nabla \cdot (\sigma_0^{n+1,exp} - \sigma_0^{n+1}) \right), \\ (\rho_0 U_0)^{n+1} - \Delta t \nabla \cdot \sigma_0^{n+1} &= \rho_0^n - \Delta t \nabla \cdot (\rho_0 U_0)^n - \Delta t \nabla p_1^{n+1}, \\ E_0^{n+1} &= E_0^n - \Delta t \frac{\gamma p_0^{n+1}}{\gamma - 1} \nabla \cdot U_0^{n+1} + \Delta t \frac{\lambda p_0^{n+1}}{R} \Delta \left( \frac{1}{\rho_0^{n+1}} \right). \end{aligned}$$

Integrating the energy equation on  $\Omega$  and using the definition (1f) of the temperature  $T_0$ , yields

$$\langle E_0^{n+1} \rangle = \langle E_0^n \rangle - \frac{\Delta t}{|\Omega|} \frac{\gamma p_0^{n+1}}{\gamma - 1} \int_{\partial\Omega} U_0^{n+1} \cdot \nu(x) d\tau(x) + \frac{\Delta t}{|\Omega|} \lambda \int_{\partial\Omega} \nabla T_0^{n+1} \cdot \nu(x) d\tau(x),$$

where  $\nu$  is the outward normal to  $\partial\Omega$  exterior to  $\Omega$  and  $d\tau$  is the measure on  $\partial\Omega$  induced by the Lebesgue measure on  $\Omega$ . Using the boundary conditions, we obtain  $\langle E_0^{n+1} \rangle = \langle E_0^n \rangle$  for all  $n \geq 0$  and by induction  $\langle E_0^n \rangle = \langle E_0^0 \rangle = \bar{E}_0 + \mathcal{O}(\Delta t^2)$  for all  $n \geq 0$ .

Now, integrating the pressure equation and using the definition (1f) of the temperature  $T$ , we obtain

$$\begin{aligned} |\Omega| \frac{p_0^{n+1}}{\gamma - 1} - \Delta t \lambda \int_{\partial\Omega} \nabla T_0^{n+1} \cdot \nu(x) d\sigma(x) &= \int_{\Omega} E_0^n dx - \Delta t \gamma \int_{\partial\Omega} E_0^n U_0^{n+1} \cdot \nu(x) d\tau(x) \\ &\quad - \Delta t^2 \int_{\partial\Omega} \frac{\gamma E_0^n}{\rho_0^{n+1}} \left( \nabla \cdot (\sigma_0^{n+1,exp} - \sigma_0^{n+1}) \right) \cdot \nu(x) d\tau(x), \end{aligned}$$

Using the boundary conditions gives

$$\frac{p_0^{n+1}}{\gamma - 1} = \langle E_0^n \rangle + \mathcal{O}(\Delta t^2) = \bar{E}_0 + \mathcal{O}(\Delta t^2).$$

Then, we proceed by induction, we prove

$$E_0^n = \bar{E}_0 + \mathcal{O}(\Delta t^2) \Rightarrow \begin{cases} E_0^{n+1} = \bar{E}_0 + \mathcal{O}(\Delta t^2), \\ \gamma \nabla \cdot U_0^{n+1} = (\gamma - 1) \frac{\lambda}{R} \Delta \left( \frac{1}{\rho_0^{n+1}} \right) + \mathcal{O}(\Delta t). \end{cases} \quad (9)$$

Indeed, since  $E_0^n = \bar{E}_0 + \mathcal{O}(\Delta t^2)$  this will conclude the proof of Lemma 1. To prove (9), we first remark that the pressure and energy equation now rewrite

$$\begin{aligned} \frac{p_0^{n+1}}{\gamma - 1} - \frac{\Delta t \lambda p_0^{n+1}}{R} \Delta \left( \frac{1}{\rho_0^{n+1}} \right) &= \bar{E}_0 - \gamma \bar{E}_0 \Delta t \nabla \cdot U_0^{n+1} + \mathcal{O}(\Delta t^2), \\ E_0^{n+1} &= \bar{E}_0 - \Delta t \gamma \bar{E}_0 \nabla \cdot U_0^{n+1} + \Delta t \frac{\lambda p_0^{n+1}}{R} \Delta \left( \frac{1}{\rho_0^{n+1}} \right) + \mathcal{O}(\Delta t^2), \end{aligned}$$

then

$$E_0^{n+1} = \frac{p_0^{n+1}}{\gamma - 1} + \mathcal{O}(\Delta t^2) = \bar{E}_0 + \mathcal{O}(\Delta t^2).$$

We conclude using another time the energy equation which gives

$$\gamma \nabla \cdot U_0^{n+1} = (\gamma - 1) \frac{\lambda}{R} \Delta \left( \frac{1}{\rho_0^{n+1}} \right) + \mathcal{O}(\Delta t).$$

□

### 2.3 Full discretization in one dimension, the first order $L^2$ -AP-scheme

The main difficulty of the spatial discretization lies in the choice of solvers for the explicit and implicit advection terms  $F_e$  and  $F_i$ . Indeed, in [24], it is proved on a model transport equation discretized with an IMEX scheme that the C.F.L. stability condition is related to the part of the flux treated explicitly, in our problem  $F_e$ , while the implicit part can be discretized using a centered or an upwind solver. Therefore, it is necessary to choose an upwinding in the solver for  $F_e$  that does not tend to 0 when  $\varepsilon$  tends to 0, otherwise, the time step, constrained by a C.F.L. condition, will also tend to 0. Following [24], we choose this upwinding to be proportional to the characteristic speeds associated to  $F_e$  (in one dimension, proportional to the largest eigenvalue of  $DF_e$ ). For the implicit term  $F_i$ , following [24], [29] or [19], we first use a centered solver. Thus, in this section, we present the full discretized AP-scheme in two dimension (for clarity) where the explicit flux  $F_e$  is discretized with a Rusanov-type solver and the implicit fluxes  $F_i$  and  $G$  with a centered solver. The resulting AP scheme gives consistent and stable results but can present oscillations near shocks, see [19]. In [24], it has been shown that these oscillations are the signature of the non  $L^\infty$  stability. Indeed, the centered solver is  $L^2$  stable but not  $L^\infty$  stable. In subsection 2.4, based on the results obtained for the Euler equations in [19, 24], we also propose a discretization where we add an upwinding on the implicit flux  $F_i$  in order to eliminate these oscillations.

In two dimension, we set  $W = (\rho, \rho u, \rho v, E)$ ,  $U = (u, v)$ ,  $\nabla \cdot F_e(W) = \partial_x F_e^x(W) + \partial_y F_e^y(W)$  where  $F_e^x(W) = (\rho u, \rho u^2, \rho u v, k_\varepsilon u)$  and  $F_e^y(W) = (\rho v, \rho u v, \rho v^2, k_\varepsilon v)$ . Similarly  $\nabla \cdot F_i(W) = \partial_x F_i^x(W) + \partial_y F_i^y(W)$  where  $F_i^x(W) = (0, p/\varepsilon, 0, h u)$  and  $F_i^y(W) = (0, 0, p/\varepsilon, h v)$ . Finally, we set  $F_e^x(W) = (F_e^x[\rho], F_e^x[\rho u], F_e^x[\rho v], F_e^x[E])$ , the same goes for the other terms  $F_e^y(W)$ ,  $F_i^x(W)$ ,  $F_i^y(W)$ .

We consider a uniform space discretization for clarity where we denote by  $\Delta x$  and  $\Delta y$  the space steps respectively in  $x$  and  $y$  direction. A cell  $C$  is labeled by the indices  $i$  and  $j$  for respectively the  $x$  and  $y$  directions. On the cell  $C_{i,j} = ((i-1)\Delta x, i\Delta x) \times ((j-1)\Delta y, j\Delta y)$ , the unknown vector of the conservative variables, is denoted by  $W_{i,j} = (\rho_{i,j}, \rho_{i,j} u_{i,j}, \rho_{i,j} v_{i,j}, E_{i,j})$  with  $U_{i,j} = (u_{i,j}, v_{i,j})$ . Then, the fully discrete scheme reads

$$\rho_{i,j}^{n+1} = \rho_{i,j}^n - \Delta t \left( \frac{\mathcal{F}_e^x[\rho]_{i+1/2,j}^n - \mathcal{F}_e^x[\rho]_{i-1/2,j}^n}{\Delta x} + \frac{\mathcal{F}_e^y[\rho]_{i,j+1/2}^n - \mathcal{F}_e^y[\rho]_{i,j-1/2}^n}{\Delta y} \right), \quad (10a)$$

$$\begin{aligned} \frac{\varepsilon}{\gamma-1} p_{i,j}^{n+1} - \Delta t^2 \left( \nabla \cdot \left( \frac{h^{n+1,exp}}{\rho^{n+1}} \nabla p^{n+1} \right) \right)_{i,j} - \frac{\varepsilon \Delta t \lambda}{R} \Delta_{dis} \left( \frac{p^{n+1}}{\rho^{n+1}} \right)_{i,j} &= \varepsilon E_{i,j}^{n+1,exp} \\ &- \varepsilon k_{i,j}^{n+1,exp} + \varepsilon^2 \Delta t \nabla_{dis} \cdot \left( \sigma^{n+1,exp} \frac{(\rho U)^{n+1,exp}}{\rho^{n+1}} \right)_{i,j} \\ &- \varepsilon \Delta t \nabla_{dis} \cdot \left( \frac{h^{n+1,exp}}{\rho^{n+1}} (\rho U)^{n+1,exp} \right)_{i,j} - \varepsilon \Delta t^2 \left( \nabla \cdot \left( \frac{h^{n+1,exp}}{\rho^{n+1}} \nabla \cdot \sigma^{n+1,exp} \right) \right)_{i,j}, \end{aligned} \quad (10b)$$

$$\begin{pmatrix} \rho_{i,j}^{n+1} & u_{i,j}^{n+1} \\ \rho_{i,j}^{n+1} & v_{i,j}^{n+1} \end{pmatrix} - \Delta t \nabla_{dis} \cdot (\sigma^{n+1})_{i,j} = \begin{pmatrix} \rho_{i,j}^{n+1} & u_{i,j}^{n+1,exp} \\ \rho_{i,j}^{n+1} & v_{i,j}^{n+1,exp} \end{pmatrix} - \frac{\Delta t}{2\varepsilon} \begin{pmatrix} \frac{p_{i+1,j}^{n+1} - p_{i-1,j}^{n+1}}{\Delta x} \\ \frac{p_{i,j+1}^{n+1} - p_{i,j-1}^{n+1}}{\Delta y} \end{pmatrix}, \quad (10c)$$

$$\begin{aligned} E_{i,j}^{n+1} &= E_{i,j}^{n+1,exp} - \Delta t \nabla_{dis} \cdot \left( \frac{\gamma p^{n+1}}{(\gamma-1)\rho^{n+1}} (\rho U)^{n+1} \right)_{i,j} \\ &+ \varepsilon \Delta t \nabla_{dis} \cdot \left( \sigma^{n+1} \frac{(\rho U)^{n+1}}{\rho^{n+1}} \right)_{i,j} + \frac{\Delta t \lambda}{R} \Delta_{dis} \left( \frac{p^{n+1}}{\rho^{n+1}} \right)_{i,j}, \end{aligned} \quad (10d)$$

where

$$\begin{aligned} (\rho u)_{i,j}^{n+1,exp} &= (\rho u)_{i,j}^n \\ &- \Delta t \left( \frac{\mathcal{F}_e^x[\rho u]_{i+1/2,j}^n - \mathcal{F}_e^x[\rho u]_{i-1/2,j}^n}{\Delta x} + \frac{\mathcal{F}_e^y[\rho u]_{i,j+1/2}^n - \mathcal{F}_e^y[\rho u]_{i,j-1/2}^n}{\Delta y} \right), \end{aligned}$$

$$\begin{aligned} (\rho v)_{i,j}^{n+1,exp} &= (\rho v)_{i,j}^n \\ &- \Delta t \left( \frac{\mathcal{F}_e^x[\rho v]_{i+1/2,j}^n - \mathcal{F}_e^x[\rho v]_{i-1/2,j}^n}{\Delta x} + \frac{\mathcal{F}_e^y[\rho v]_{i,j+1/2}^n - \mathcal{F}_e^y[\rho v]_{i,j-1/2}^n}{\Delta y} \right), \end{aligned}$$

$$E_{i,j}^{n+1,exp} = E_{i,j}^n - \Delta t \left( \frac{\mathcal{F}_e^x[E]_{i+1/2,j}^n - \mathcal{F}_e^x[E]_{i-1/2,j}^n}{\Delta x} + \frac{\mathcal{F}_e^y[E]_{i,j+1/2}^n - \mathcal{F}_e^y[E]_{i,j-1/2}^n}{\Delta y} \right),$$

with  $\rho_{i,j}^{n+1,exp} = \rho_{i,j}^{n+1}$  and where for the explicit numerical fluxes  $(\mathcal{F}_e^x)^n$ , we consider a Rusanov solver:

$$(\mathcal{F}_e^x[m])_{i+1/2,j}^n := \frac{(F_e^x[m])_{i+1,j}^n + (F_e^x[m])_{i,j}^n}{2} - (\mathcal{D}_e^x)_{i+1/2,j}^n (m_{i+1,j}^n - m_{i,j}^n),$$

for  $m = \rho, u, v$  or  $E$  and where  $(\mathcal{D}_e^x)_{i+1/2,j}^n$  the explicit viscosity coefficient, is taken as half of the maximum explicit eigenvalue of the Jacobian matrix associated to  $(F_e^x)^n$ :

$$(\mathcal{D}_e^x)_{i+1/2,j}^n = \frac{1}{2} \max(|u_{i+1,j}^n|, |u_{i,j}^n|).$$

Likewise, in the  $y$  direction the explicit fluxes  $(\mathcal{F}_e^y)^n$  are given by

$$(\mathcal{F}_e^y[m])_{i,j+1/2}^n := \frac{(F_e^y[m])_{i,j+1}^n + (F_e^y[m])_{i,j}^n}{2} - (\mathcal{D}_e^y)_{i,j+1/2}^n (m_{i,j+1}^n - m_{i,j}^n),$$

where  $(\mathcal{D}_e^y)_{i,j+1/2}^n$  the explicit viscosity coefficient, is taken as half of the maximum explicit eigenvalue of the Jacobian matrix associated to  $(F_e^y)^n$ :

$$(\mathcal{D}_e^y)_{i,j+1/2}^n = \frac{1}{2} \max(|v_{i,j+1}^n|, |v_{i,j}^n|).$$

Let us note that the upwindings depend only on the fluid velocity.

For all vector  $F = (F^x, F^y)$ ,  $\nabla_{dis} \cdot F_{i,j}$  is defined with a centered approximation:

$$\nabla_{dis} \cdot F_{i,j} = \frac{F_{i+1,j}^x - F_{i-1,j}^x}{2 \Delta x} + \frac{F_{i,j+1}^y - F_{i,j}^y}{2 \Delta y}.$$

The discrete Laplacian operator is classically defined by

$$\begin{aligned} \left(\frac{p^{n+1}}{\rho^{n+1}}\right)_{i,j} &= \frac{\left(\frac{p^{n+1}}{\rho^{n+1}}\right)_{i+1,j} - 2 \left(\frac{p^{n+1}}{\rho^{n+1}}\right)_{i,j} + \left(\frac{p^{n+1}}{\rho^{n+1}}\right)_{i-1,j}}{\Delta x^2} \\ &\quad + \frac{\left(\frac{p^{n+1}}{\rho^{n+1}}\right)_{i,j+1} - 2 \left(\frac{p^{n+1}}{\rho^{n+1}}\right)_{i,j} + \left(\frac{p^{n+1}}{\rho^{n+1}}\right)_{i,j-1}}{\Delta y^2}. \end{aligned}$$

Finally for all real functions  $\alpha$  and  $f$ , the quantity  $(\nabla(\alpha \nabla f))_{i,j}$  is defined by

$$\begin{aligned} (\nabla(\alpha \nabla f))_{i,j} &= \frac{1}{\Delta x} \left( \frac{\alpha_{i+1,j} + \alpha_{i,j}}{2} \frac{f_{i+1,j} - f_{i,j}}{\Delta x} - \frac{\alpha_{i,j} + \alpha_{i-1,j}}{2} \frac{f_{i,j} - f_{i-1,j}}{\Delta x} \right) \\ &\quad + \frac{1}{\Delta y} \left( \frac{\alpha_{i,j+1} + \alpha_{i,j}}{2} \frac{f_{i,j+1} - f_{i,j}}{\Delta y} - \frac{\alpha_{i,j} + \alpha_{i,j-1}}{2} \frac{f_{i,j} - f_{i,j-1}}{\Delta y} \right). \end{aligned}$$

In the following, the scheme (10) is called ‘‘First order  $L^2$  AP scheme’’.

## 2.4 The first order implicit upwinding

As mentioned before, choosing a centered discretization for the implicit inviscid flux  $F_i$  leads to an  $L^2$  stable scheme. In some cases, we may want to add some stabilization with the help of upwinding to reduce appearing spurious oscillations. Adding numerical dissipation on the implicit inviscid flux, we are able to construct an order 1  $L^\infty$  stable scheme [24]. For that, we compute the  $L^2$  stable solution  $W_{i,j}^{n+1,L^2}$  with the ‘‘First order  $L^2$  AP scheme’’ (10) and we add an upwinding as done for the explicit numerical

flux  $(\mathcal{F}_e)_{j+1/2}^n$ , thus leading to the “First order  $L^\infty$  AP scheme”.

$$\begin{aligned}
W_{i,j}^{n+1} &= W_{i,j}^{n+1,L2} \\
&+ \frac{\Delta t}{\Delta x} \left( (\mathcal{D}_i^x)_{i+1/2,j}^n (W_{i+1,j}^{n+1} - W_{i,j}^{n+1}) - (\mathcal{D}_i^x)_{i-1/2,j}^n (W_{i,j}^{n+1} - W_{i-1,j}^{n+1}) \right) \\
&+ \frac{\Delta t}{\Delta y} \left( (\mathcal{D}_i^y)_{i,j+1/2}^n (W_{i,j+1}^{n+1} - W_{i,j}^{n+1}) - (\mathcal{D}_i^y)_{i,j-1/2}^n (W_{i,j}^{n+1} - W_{i,j-1}^{n+1}) \right).
\end{aligned} \tag{11a}$$

where  $(\mathcal{D}_i^x)_{i,j+1/2}^n$  and  $(\mathcal{D}_i^y)_{i,j+1/2}^n$  are the implicit viscosity coefficients, taken as half of the maximum implicit eigenvalues of  $DF_i^x$  and  $DF_i^y$ :

$$(\mathcal{D}_i^x)_{i+1/2,j}^n = \frac{1}{2} \max (|\lambda_i^x(W_{i+1,j}^n)|, |\lambda_i^x(W_{i,j}^n)|), \tag{11b}$$

$$(\mathcal{D}_i^y)_{i,j+1/2}^n = \frac{1}{2} \max (|\lambda_i^y(W_{i,j+1}^n)|, |\lambda_i^y(W_{i,j}^n)|), \tag{11c}$$

where  $|\lambda_i^x(W)| = |u|/2 + \sqrt{u^2/4 + c^2/\varepsilon}$  and  $|\lambda_i^y(W)| = |v|/2 + \sqrt{v^2/4 + c^2/\varepsilon}$ .

The upwinding must be applied after the computation of all conservative variables. Moreover, it is important to note that the viscosity coefficients  $(\mathcal{D}_i^x)$  and  $(\mathcal{D}_i^y)$  depend on the scaling parameter  $\varepsilon$  inversely proportional to the Mach number and may lead to excessive diffusion in the low Mach number regime. Therefore, the proposed stabilization technique is used only if needed, depending on the problem to solve. We refer to this modified scheme (11) as the “First order  $L^\infty$  AP scheme”. In Figure 1, we compare the density profiles for a 2D Riemann problem (see Section 4.1 for its description) computed with the “First order  $L^2$  AP scheme” (left) against the “First order  $L^\infty$  AP scheme” (right). As expected, with an upwinding on the implicit flux we are able to eliminate the oscillations appearing when a centered discretization for the implicit part is chosen. However, the solution is also more diffused and it shows the need to extend the schemes to a higher order of accuracy.

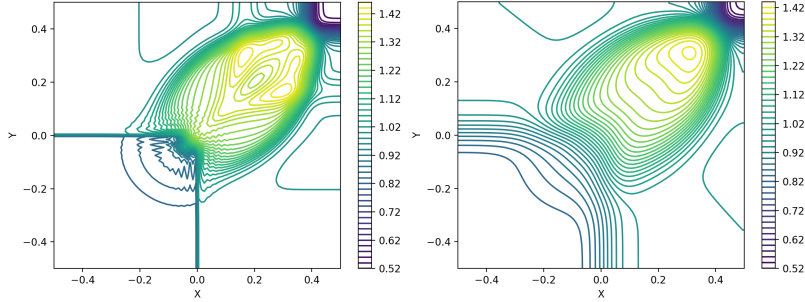


**Fig. 1** 2D Riemann problem (see Section 4.1 for its description): Density isolines given by the “First order  $L^2$  AP scheme” (left) and by the “First order  $L^\infty$  AP scheme” (right).

## 2.5 Asymptotic stability : C.F.L. condition on the time step

In [19], we considered the full Euler equations, i.e. with  $\mu = \lambda = 0$ , and we conducted a one-dimensional linear Fourier stability analysis of the first order AP schemes (“First order  $L^2$  AP scheme” and “First order  $L^\infty$  AP scheme”). We proved on a linearized system that our “First order  $L^2$  AP scheme” (10) is stable under the C.F.L. condition  $\gamma\Delta t = |u|\Delta x$ . Furthermore, when adding the implicit upwinding on the implicit inviscid part, our “First order  $L^\infty$  AP scheme” (11) is stable under the C.F.L. condition  $\Delta t = |u|\Delta x$ . Then, both discretizations are linearly asymptotically stable. The time step restriction does not depend on the Mach number and is only related to the fluid velocity.

Moreover, we show numerically that the situation does not change in case of viscous flows. In Figure 2, we compare the time step sizes  $\Delta t$  used for different schemes for the first problem of Stokes (see Section 4.3 for its description) for which  $\varepsilon = 10^{-6}$ . On the left figure, we compare the time step sizes between the explicit scheme and the first order AP schemes. We observe that the time steps of the “First order  $L^2$  AP scheme” with an explicit discretization of the viscous terms are around  $1/\sqrt{\varepsilon} = 10^3$  times bigger than the ones required by the fully explicit scheme. With an implicit discretization of the viscous terms, the time steps sizes of our “First order  $L^2$  AP scheme” and “First order  $L^\infty$  AP scheme” are bigger due to the diffusion stability condition. This shows that the AP schemes can employ time step sizes independently of the Mach number regime. On the right figure, we observe the advantages of an implicit discretization of the viscous terms in the case of highly viscous flows.

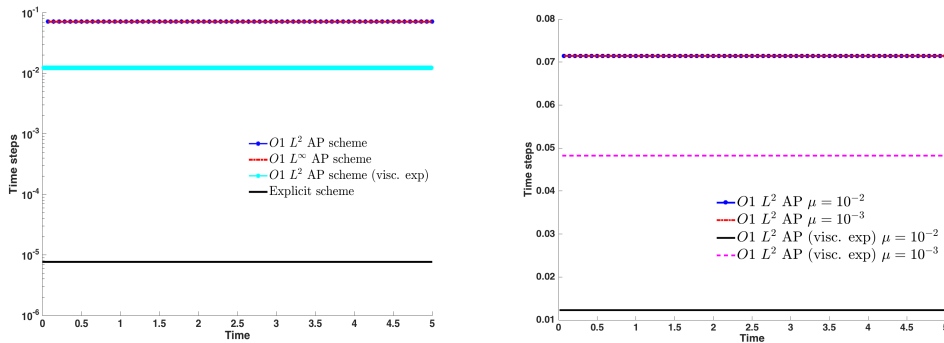


**Fig. 2** Time step sizes  $\Delta t$  as a function of time for the first problem of Stokes (see Section 4.3 for its description): Left panel: Comparison of the Order 1 AP schemes against the explicit scheme for  $\varepsilon = 10^{-6}$  and  $\mu = 10^{-2}$ . Right panel: Comparison of the Order 1  $L^2$  AP scheme against the Order 1  $L^2$  AP scheme with an explicit discretization of the viscous terms for  $\varepsilon = 10^{-6}$  and with  $\mu = 10^{-2}$  and  $\mu = 10^{-3}$ .

## 3 The second order AP-schemes

The second-order extension of the schemes is a necessary step because some test cases require more precision than a first-order scheme can provide. The extension to

the second order accuracy in time is done with an Implicit-Explicit (IMEX) Runge-Kutta approach [17, 18, 23]. We choose the scheme proposed in [17] called in the sequel ARS discretization like in [19, 29, 29]. This second-order semi-discretization has the advantage of requiring the calculation of only one intermediate state while other second-order semi-discretizations would require calculating two. This scheme has been originally constructed for convection-diffusion equations with an implicit treatment for the diffusion terms. The Butcher tableau relative to the considered ARS scheme is detailed in Table 1 with  $\beta = 1 - \sqrt{2}/2$ . Note that on the left is reported the explicit tableau applied to the flux  $F_e$  while on the right the implicit tableau applied to the flux  $F_i$ .

0	0	0	0
$\beta$	$\beta$	0	0
1	$\beta - 1$	$2 - \beta$	0
	$\beta - 1$	$2 - \beta$	0

0	0	0	0
$\beta$	0	$\beta$	0
1	0	$1 - \beta$	$\beta$
	0	$1 - \beta$	$\beta$

**Table 1** Butcher tableaux for the ARS(2,2,2) time discretization. Left panel: explicit tableau. Right panel: implicit tableau.

Using the ARS discretization and considering that the implicit part is given by the fast convective flux  $F_i$  and the diffusion part  $G$ , we obtain the following AP-semi-discretization of the Navier-Stokes system:

$$\frac{W^* - W^n}{\Delta t} + \beta \nabla \cdot F_e(W^n) + \beta \nabla \cdot F_i(W^*) = \beta \nabla \cdot G(W^*, \nabla W^*), \quad (12a)$$

$$\frac{W^{n+1} - W^n}{\Delta t} + (\beta - 1) \nabla \cdot F_e(W^n) + (2 - \beta) \nabla \cdot F_e(W^*) \quad (12b)$$

$$\begin{aligned} &+ (1 - \beta) \nabla \cdot F_i(W^*) + \beta \nabla \cdot F_i(W^{n+1}) \\ &= (1 - \beta) \nabla \cdot G(W^*, \nabla W^*) + \beta \nabla \cdot G(W^{n+1}, \nabla W^{n+1}), \end{aligned} \quad (12c)$$

with  $\beta = 1 - 1/\sqrt{2}$ .

Then, we proceed as for the first-order scheme, but at each step. That is to say, for Step 1, we first reformulate the energy equation into an equation for the pressure, in which we insert the momentum equation (see Eq. (6)), and then we approximate the implicit quantities  $k_\varepsilon^*$ ,  $h^*$ ,  $\sigma^*$  and  $(\sigma U)^*$  by their explicit convected values  $k_\varepsilon^{*,exp} = k_\varepsilon(W^{*,exp})$ ,  $h^{*,exp} = h(W^{*,exp})$ ,  $\sigma^{*,exp} = \sigma(W^{*,exp})$  and  $(\sigma U)^{*,exp} = (\sigma(W^{*,exp})U^{*,exp})$ . We do the same for Step 2. Doing so, we obtain linear equations for the pressures  $p^*$  and  $p^{n+1}$ .

The second order AP semi-discretization in time is then given by

Step 1:

$$\rho^\star = \rho^n - \beta \Delta t \nabla \cdot (\rho^n U^n), \quad (13a)$$

$$\begin{aligned} \frac{\varepsilon}{\gamma - 1} p^\star - \beta^2 \Delta t^2 \nabla \cdot \left( \frac{h^{\star,exp}}{\rho^\star} \nabla p^\star \right) - \frac{\varepsilon \beta \Delta t \lambda}{R} \Delta \left( \frac{p^\star}{\rho^\star} \right) &= \varepsilon (E^{\star,exp} - k^{\star,exp}) \\ - \varepsilon \beta \Delta t \left( \nabla \cdot \left( \frac{h^{\star,exp}}{\rho^\star} (q^{\star,exp} - \beta \Delta t \nabla \cdot \sigma^{\star,exp}) \right) - \varepsilon \nabla \cdot \left( \sigma^{\star,exp} \frac{q^{\star,exp}}{\rho^\star} \right) \right), \end{aligned} \quad (13b)$$

$$q^\star - \beta \Delta t \nabla \cdot \sigma^\star = q^{\star,exp} - \beta \Delta t \frac{1}{\varepsilon} \nabla p^\star, \quad (13c)$$

$$E^\star = E^{\star,exp} - \beta \Delta t \left( \nabla \cdot \left( \frac{\gamma p^\star}{(\gamma - 1) \rho^\star} q^\star \right) - \varepsilon \nabla \cdot \left( \sigma^\star \frac{q^\star}{\rho^\star} \right) - \frac{\lambda}{R} \Delta \left( \frac{p^\star}{\rho^\star} \right) \right), \quad (13d)$$

where  $(\rho U)^\star, exp = (\rho U)^n - \beta \Delta t \nabla \cdot (\rho^n U^n \otimes U^n)$  and  $E^{\star,exp} = E^n - \beta \Delta t \nabla \cdot (k_\varepsilon^n U^n)$ .

Step 2:

$$\begin{aligned} W^{n+1,exp} = W^n - \Delta t ((\beta - 1) \nabla \cdot F_e(W^n) + (2 - \beta) (\nabla \cdot F_e(W^\star))) \\ + \Delta t ((1 - \beta) (\nabla \cdot F_i(W^\star) - G(W^\star))). \end{aligned} \quad (14a)$$

$$\rho^{n+1} = \rho^n - \Delta t (\beta - 1) \nabla \cdot (\rho^n U^n) - \Delta t (2 - \beta) \nabla \cdot (\rho^\star U^\star), \quad (14b)$$

$$\begin{aligned} \frac{\varepsilon}{\gamma - 1} p^{n+1} - \beta^2 \Delta t^2 \nabla \cdot \left( \frac{h^{n+1,exp}}{\rho^{n+1}} \nabla p^{n+1} \right) - \frac{\varepsilon \beta \Delta t \lambda}{R} \Delta \left( \frac{p^{n+1}}{\rho^{n+1}} \right) = \\ \varepsilon (E^{n+1,exp} - k_\varepsilon^{n+1,exp}) - \varepsilon \beta \Delta t \nabla \cdot \left( \frac{h^{n+1,exp}}{\rho^{n+1}} (q^{n+1,exp} + \beta \Delta t \nabla \cdot \sigma^{n+1,exp}) \right) \\ + \varepsilon^2 \beta \Delta t \nabla \cdot \left( \sigma^{n+1,exp} \frac{q^{n+1,exp}}{\rho^{n+1}} \right), \end{aligned} \quad (14c)$$

$$q^{n+1} - \beta \Delta t \nabla \cdot \sigma^{n+1} = q^{n+1,exp} - \frac{\beta \Delta t}{\varepsilon} \nabla p^{n+1}, \quad (14d)$$

$$E^{n+1} = E^{n+1,exp} - \beta \Delta t \nabla \cdot \left( \frac{\gamma p^{n+1}}{(\gamma - 1) \rho^{n+1}} q^{n+1} \right) + \frac{\beta \Delta t \lambda}{R} \Delta \left( \frac{p^{n+1}}{\rho^{n+1}} \right). \quad (14e)$$

We recall that  $k^l = k(W^l)$ ,  $h^l = h(W^l) = \gamma(E^l - k^l)$  and  $\sigma^l = \sigma(W^l)$  for  $l = \star, exp$  or  $n + 1, exp$ .

For the extension to the second order space accuracy, we first remark that the discretizations of the viscous terms are already of second order, then we do not modify their discretizations. For the implicit flux, if we consider the ‘‘First order  $L^2$  scheme’’, the centered approximations of implicit terms are also of second order. Then, we only need to handle the discretized explicit flux terms with the Ruzanov solver. We classically use the MUSCL technique [31] for the convective terms and so a piecewise linear reconstruction of  $W_j^n$ :

$$\widehat{W}_{i,j}^n(x, y) = W_{i,j}^n + (\alpha^x)_{i,j}^n (x - x_i) + (\alpha^y)_{i,j}^n (y - y_j),$$

where  $x_i = (i - 1/2) \Delta x$ ,  $y_j = (j - 1/2) \Delta y$ ,  $(\alpha^x)_{i,j}^n$  and  $(\alpha^y)_{i,j}^n$  are limited slopes and are computed for each component using a minmod limiter:

$$(\alpha^x)_{i,j}^n = \text{minmod} \left( \frac{W_{i+1,j} - W_{i,j}}{\Delta x}, \frac{W_{i,j} - W_{i-1,j}}{\Delta x} \right),$$

the slope in the  $y$  direction,  $(\alpha^y)_{i,j}^n$ , is computed in the same manner and where the limiter is defined to pick out the flattest slope when they have the same sign:

$$\text{minmod}(a, b) = \frac{1}{2} (\text{sign}(a) + \text{sign}(b)) \min(|a|, |b|) = \begin{cases} a & \text{if } |a| < |b|, ab > 0, \\ b & \text{if } |b| < |a|, ab > 0, \\ 0 & \text{otherwise.} \end{cases}$$

This piecewise linear reconstruction is used for defining the explicit numerical fluxes at the interfaces. Using the notations introduced for the first order scheme, the numerical flux in the  $x$  direction is given by

$$(\mathcal{F}_e^x)_{i+1/2,j}^n = \frac{F_e^x(W_{(i+1,-),j}^n) + F_e^x(W_{(i,+),j}^n)}{2\Delta x} - (\mathcal{D}_e^x)_{i+1/2,j}^n (W_{(i+1,-),j}^n - W_{(i,+),j}^n), \quad (15)$$

where  $(\mathcal{D}_e^x)_{i+1/2,j}^n = \frac{1}{2} \max(|u_{(i,+),j}^n|, |u_{(i+1,-),j}^n|)$  and

$$W_{(i,\pm),j}^n = \widehat{W}_{i,j}^n \left( x_i \pm \frac{1}{2} \Delta x \right) = W_{i,j}^n \pm \frac{\Delta x}{2} (\alpha^x)_{i,j}^n.$$

The numerical flux in the  $y$  direction is calculated in the same way. The resulting scheme given by (13), (14) in time and (15) is called in the following ‘‘Second order  $L^2$  AP scheme’’.

For the implicit upwinding, it is sufficient to add numerical diffusion on the implicit flux  $F_i$  only at the end of the second step of (14). Adding it in both steps would imply a higher computational cost for similar results. As done for the first order scheme, we compute the  $L^2$  stable solution  $W_j^{n+1,L2}$  with (13), (14), (15) and then add numerical dissipation on the conservative variables:

$$\begin{aligned} W_{i,j}^{n+1} &= W_{i,j}^{n+1,L2} \\ &+ \frac{\Delta t}{\Delta x} \left( (\tilde{\mathcal{D}}_i^x)_{i+1/2,j}^n (\tilde{W}_{(i+1,-),j}^{n+1} - \tilde{W}_{(i,+),j}^{n+1}) - (\tilde{\mathcal{D}}_i^x)_{i-1/2,j}^n (\tilde{W}_{(i,-),j}^{n+1} - \tilde{W}_{(i-1,+),j}^{n+1}) \right) \\ &+ \frac{\Delta t}{\Delta y} \left( (\tilde{\mathcal{D}}_i^y)_{i,j+1/2}^n (\tilde{W}_{i,(j+1,-)}^{n+1} - \tilde{W}_{i,(j,+)}^{n+1}) - (\tilde{\mathcal{D}}_i^y)_{i,j-1/2}^n (\tilde{W}_{i,(j,-)}^{n+1} - \tilde{W}_{i,(-1,+),j}^{n+1}) \right). \end{aligned} \quad (16)$$

where  $(\tilde{\mathcal{D}}_i^x)_{i+1/2,j}^n = 1/2 \max(|\lambda_i^x(\tilde{W}_{(i+1,-),j}^n)|, |\lambda_i^x(\tilde{W}_{(i,+),j}^n)|)$  and  $\tilde{W}_{(i,\pm),j}^{n+1} = W_{i,j}^{n+1} \pm \frac{\Delta x}{2} (\alpha^x)_{i,j}^n$ . Remark that the slopes and the viscosity coefficients are explicit, then the scheme is linear. The implicit viscosity coefficient in the  $y$  direction is calculated in the same manner.

Let us note that, see [24], IMEX methods of order higher than one for hyperbolic problems cannot be TVD nor  $L^\infty$  stable for unconstrained time steps [24, 32]. Thus, the scheme given by (13), (14) in time and (15), (16) in space, is still only  $L^2$  stable but the oscillations are reduced thanks to the upwinding on the implicit part. We now refer to this scheme as the “Second order  $L^{2,stab}$  AP scheme”.

## 4 Numerical simulations

In this section, we present several numerical test cases which show the good behavior of our AP schemes. Results are shown depending on the numerical test, for the “Second order  $L^2$  AP scheme and the “Second order  $L^{2,stab}$  AP scheme”.

The numerical test cases chosen are in two dimensions and involve, except for the first one, the Navier-Stokes equations in both compressible and incompressible regimes. The first one test-case involve the Euler equations.

If not mentioned, the specific gas constant  $R$  is set to 1 ( $c_v = 2.5$ ), the adiabatic constant  $\gamma$  to 1.4 and the time step size is given by

$$\Delta t^n = C \frac{1}{\frac{\gamma \max_{i,j} |u_{i,j}^n|}{\Delta x} + \frac{\gamma \max_{i,j} |v_{i,j}^n|}{\Delta y}}, \quad (17)$$

where the constant  $C = 0.45$ .

Finally, it is important to note that the non-rescaled Navier-Stokes system is obtained by setting  $\varepsilon = 1$  in the rescaled system (2). Thus, if for a given test-case,  $\varepsilon$  is set to 1, this does not mean that the incompressible regime is not reached in certain regions of the domain. Indeed, the physical Mach number given by

$$M = \sqrt{\varepsilon} \frac{|U|}{c} = \frac{\sqrt{u^2 + v^2}}{\sqrt{\frac{\gamma p}{\varepsilon \rho}}}. \quad (18)$$

varies within the domain and can reach very small values.

### 4.1 2D Riemann problem

We consider a two-dimensional Riemann problem introduced in [33]. We set  $\Omega = [-0.5, 0.5]^2$  and transmissive boundary conditions ( $\nabla W \cdot \nu = 0$ ). The initial data consists in four constant states defined in four quadrants:

$$(\rho, u, v, p)(0, x, y) = \begin{cases} (1, 0.726, 0, 1) & \text{if } x \leq 0, y > 0, \\ (0.5313, 0, 0, 0.4) & \text{if } x \geq 0, y > 0, \\ (0.8, 0, 0, 1) & \text{if } x \leq 0, y \leq 0, \\ (1, 0, 0.726, 1) & \text{if } x \geq 0, y \leq 0. \end{cases} \quad (19)$$

We set  $\varepsilon = 1$ ,  $\mu = \lambda = 0$  and the final time is  $t_{end} = 0.25$ .

This configuration is referred to as 2DR98 “*configuration F*” in [33]. It is constituted of two shocks moving respectively towards the right and top of the domain and two steady contact discontinuities in the bottom left part of the domain.

In Figure 3, we display the density contour plots and isolines at the final time computed with the “Second order  $L^2$  AP scheme (top) and the “Second order  $L^{2,stab}$  AP scheme” (bottom). They are in good agreement with the reference solution given

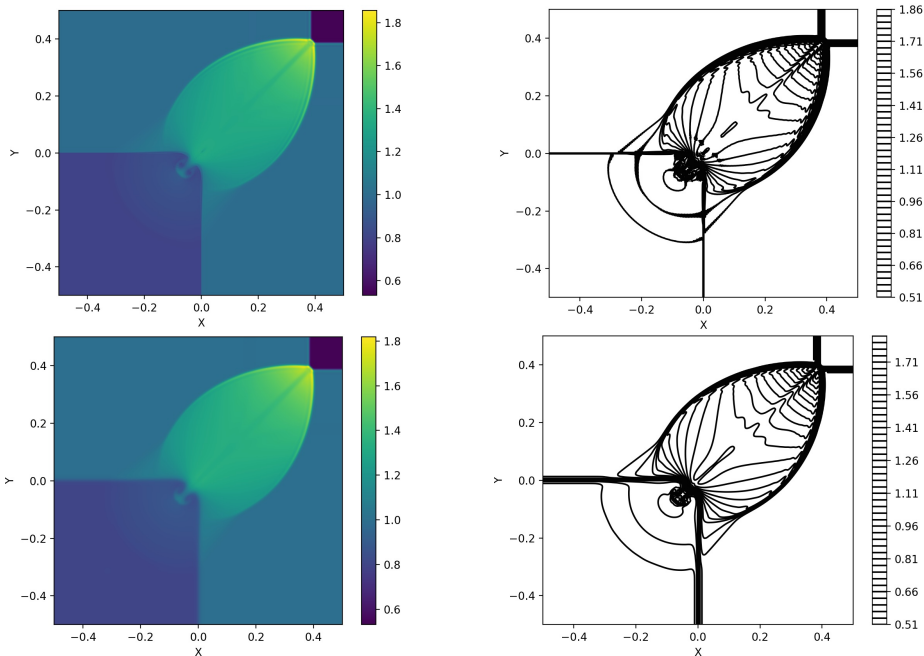


**Fig. 3** 2D Riemann problem . Density contour plots (left) and density isolines (right). On the top: “Second order  $L^2$  AP scheme”, on the bottom: “Second order  $L^{2,stab}$  AP scheme”.

in [33]. With both schemes the contact discontinuities are preserved and do not move with time. Furthermore, the interface computed with the  $L^2$  AP scheme (when no implicit diffusion is added) is much sharper. However, looking at the isolines we see that the  $L^2$  AP presents some spurious oscillations (top right) that do not appear when the stabilization procedure is applied (bottom right).

In Figure 4, we present, the Mach number distribution calculated at each point with (18), the pressure and the velocity components. The Mach number ranges between 0 and 1.14 in all the domain and for all times. We also confirm that the normal velocities and pressure have stayed constant along the contact discontinuities.

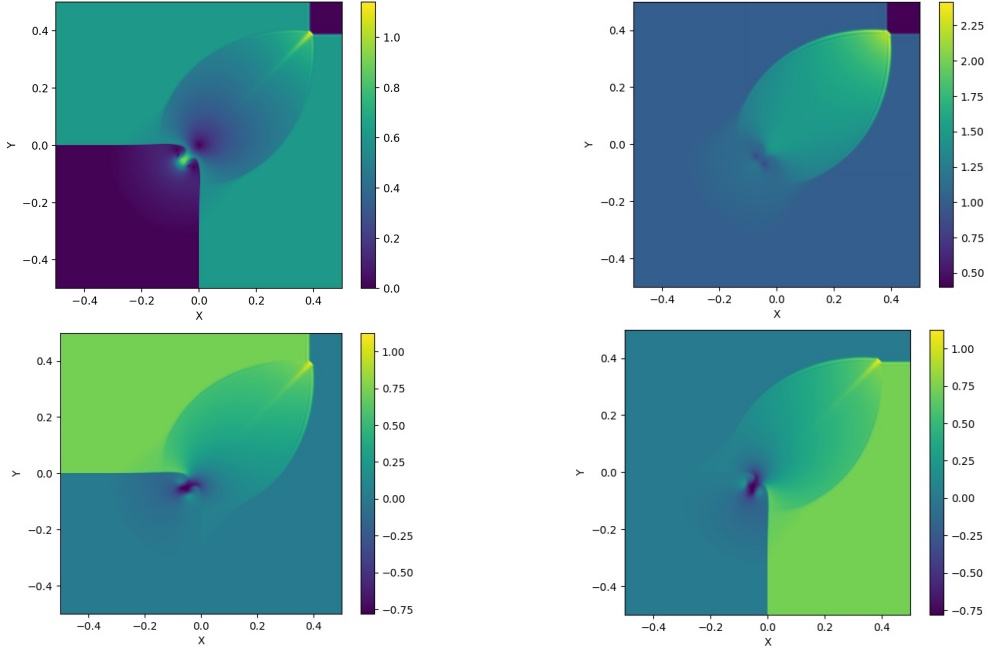


**Fig. 4** 2D Riemann problem. Top left: physical Mach number, top right: pressure, bottom left  $u$  velocity and bottom right:  $v$  velocity, contour plots at time  $t = 0.25$  given by the “Second order  $L^2$  AP scheme” for  $400 \times 400$  cells.

## 4.2 Explosion problem

We consider the explosion problem proposed by [11] where we set  $\Omega = [-1, 1]^2$  and Dirichlet boundary conditions given by the initial condition (20) during all the simulation. Initially the fluid is at rest, with a higher density and pressure at the center of the domain, inside the circle of radius 0.4 and centered in  $(0, 0)$ . The initial states are given by

$$(\rho, p)(0, x, y) = \begin{cases} (1, 1) & \text{if } r < 0.4, \\ (0.125, 0.1) & \text{otherwise,} \end{cases} \quad (u, v)(0, x, y) = (0, 0), \quad (20)$$

where  $r = \sqrt{x^2 + y^2}$ ,  $\varepsilon = 1$ ,  $\lambda = 0$ ,  $t_{end} = 0.25$  and different values of  $\mu$ . In the inviscid case, when  $\mu = 0$ , since the flow is axi-symmetric, the reference radial solution can be computed solving a one-dimensional inhomogeneous system (see [11] for more details). We solve it using a second order explicit scheme with a Rusanov-type solver on a refined grid ( $N = 5000$ ) which gives a reference solution for  $\mu = 0$ .

In Figure 5, we compare the results given by the “Second order  $L^2$  AP scheme” (squares) against the “Second order  $L^2$  AP scheme” but with an explicit discretization for the viscous terms (crosses). Results are displayed for  $\mu = 10^{-2}$  and  $10^{-3}$ . Looking at the profiles, we obtain the same results independently of the discretization and we can observe the convergence towards the inviscid reference solution when  $\mu$  tends to 0.

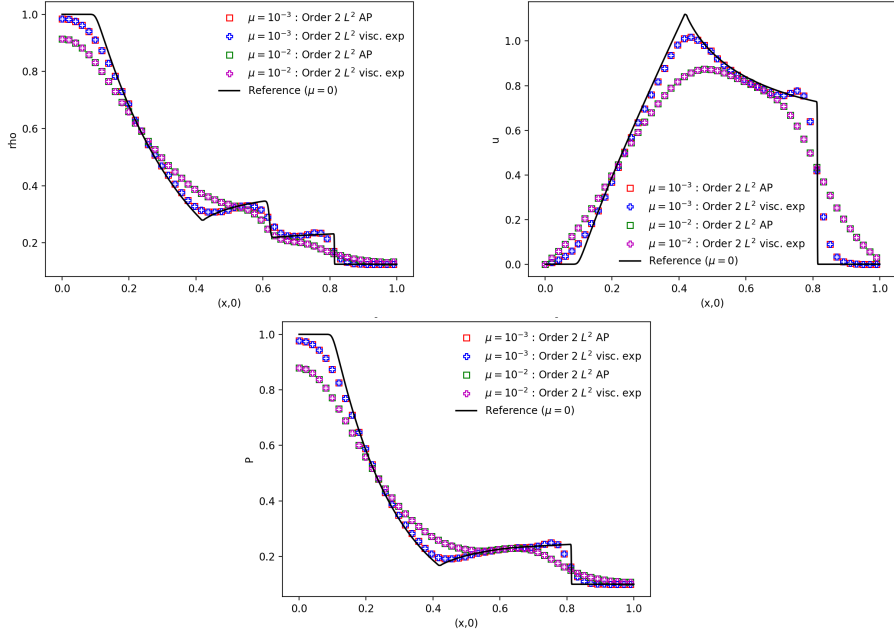


**Fig. 5** Explosion problem:  $u$  velocity (top left),  $v$  velocity (top right) and pressure (bottom) one-dimensional cuts at time  $t = 0.25$  and  $100 \times 100$  points. Comparison between an implicit and explicit discretization of the viscous terms for the “Second order  $L^2$  AP scheme”.

Moreover, as expected, Table 2 shows the advantage on the time step size of treating implicitly the viscous part. For  $\mu = 10^{-2}$ , the implicit discretization allows a time step that is 5.6 times bigger than with an explicit treatment.

Scheme	Number of times steps		
	$\mu = 0$	$\mu = 10^{-3}$	$\mu = 10^{-2}$
Second order $L^2$ AP	73	69	58
Second order $L^2$ AP (visc. exp)	73	96	330

**Table 2** Explosion problem: Number of time steps for various viscous regimes on a  $101 \times 101$  grid. Comparison between an implicit and explicit discretization of the viscous flux for the “Second order  $L^2$  AP scheme”.

### 4.3 First problem of Stokes

We simulate a test problem for which an analytical solution is known. In Stokes’s first problem [34], we consider an incompressible viscous fluid in a semi-infinite plate. The fluid is at rest and then a constant velocity is set at  $y = 0$ . The fluid is brought into motion by the action of the viscous stress at the bottom. Here we set  $\Omega = [0, 1] \times [0, 2]$

and the initial data are given by:

$$\rho(0, x, y) = 1, \quad u(0, x, y) = \begin{cases} U & \text{if } y = 0, \\ 0 & \text{otherwise,} \end{cases} \quad v(0, x, y) = 0, \quad p(0, x, y) = 1, \quad (21)$$

with  $U = 1$ ,  $\varepsilon = 10^{-6}$  and  $\lambda = 0$ . For a semi-infinite plate, the exact solution of the problem is

$$u(x, y, t) = U \left( 1 - \operatorname{erf} \left( \frac{y}{2\sqrt{\gamma\mu}} \right) \right), \quad (22)$$

with constant density, pressure and velocity  $v$ .

For the simulations we consider periodic boundary conditions on the  $x$  direction and Dirichlet boundary conditions on the  $y$  direction. In particular we set the exact solution given by (22) for the velocity  $u$  and the initial condition for the other variables.

We run the simulations with the “Second order  $L^2$  AP scheme” until the final time  $t_{end} = 30$  with  $5 \times 100$  points and we choose different values for the viscosity coefficients  $\mu = 10^{-1}$  and  $\mu = 10^{-3}$ .

In Figures 6 and 7, we show for each coefficient the  $u$  velocity contour plot at the final time (left) and compare our solution against the exact solution at different time levels (right). We compare it plotting the  $u$  velocity versus the wall distance. As expected, the disturbance caused by the impulsive motion of the boundary diffuses into the fluid as time progresses and faster when  $\mu$  is bigger.

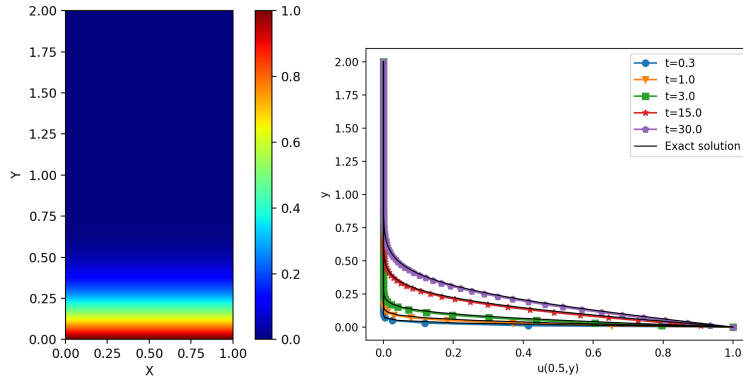


**Fig. 6** Stokes first problem: Results for the viscosity coefficients  $\mu = 10^{-3}$  with  $5 \times 100$  cells. Left:  $u$ -distribution contour plot at  $t_{end} = 30$ . Right: Comparison of the  $u$  velocity versus the wall distance against the exact solution at times  $t = 0.3, 1.0, 3, 15$  and  $30$ .

#### 4.4 Double shear layer: Incompressible solution

We consider a test case studied in [35] which consists of a double shear layer in a periodic domain. It is used to validate the asymptotic consistency of our scheme since for small values of  $\varepsilon$  the solution is close to the incompressible solution. We set  $\Omega = [0, 1]^2$  and periodic boundary conditions everywhere. The initial data are well

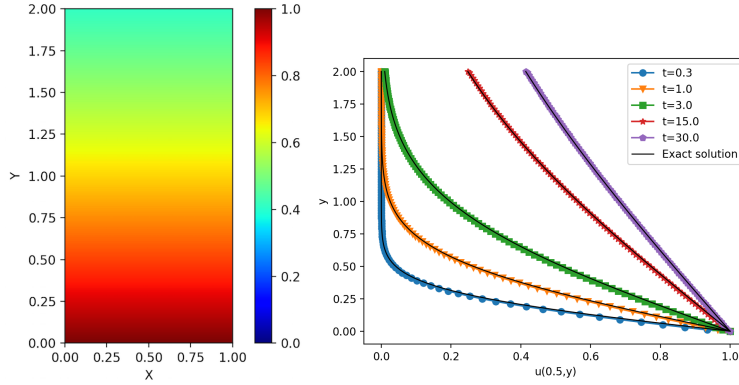


**Fig. 7** Stokes first problem: Results for the viscosity coefficients  $\mu = 10^{-1}$  (bottom) with  $5 \times 100$  points. Left:  $u$ -distribution contour plot at  $t_{end} = 30$ . Right: Comparison of the  $u$  velocity versus the wall distance against the exact solution at times  $t = 0.3, 1.0, 3, 15$  and  $30$ .

prepared to the incompressible regime (divergence free velocity field and constant pressure) and are given by:

$$\begin{aligned} \rho(0, x, y) &= 1, & u(0, x, y) &= \begin{cases} \tanh(30(y - 0.25)) & \text{if } y < 0.5, \\ \tanh(30(0.75 - y)) & \text{otherwise,} \end{cases} \\ v(0, x, y) &= 0.05 \sin(2\pi x), & p(0, x, y) &= 1, \end{aligned} \quad (23)$$

where  $\lambda = 0$ . The shear layer is initially perturbed by a vertical velocity of small amplitude. Then, each of the layers will evolve into large vortices and will be thinned between those rolls. One relevant quantity is the vorticity  $w = \partial_x v - \partial_y u$ , which we compute using a second order difference approximation.

$$w_{i,j} = \frac{v_{i+1,j} - v_{i-1,j}}{2\Delta x} - \frac{u_{i,j+1} - u_{i,j-1}}{2\Delta y}. \quad (24)$$

In Figure 8, we show the contour vorticity plots for  $\mu = 2 \cdot 10^{-4}$  and  $\varepsilon = 10^{-3}$  at different times. The “Second order  $L^2$  AP scheme” well captures the incompressible solution (see [35]).

## 4.5 Heat conduction

In order to validate our scheme in the presence of heat conduction, we consider the following problem proposed by [36, 37]. We consider a fluid initially at rest, with a higher density at the center of the domain, inside the circle of radius 0.2 and centered in  $(0, 0)$ . The initial states are given by

$$\rho(0, x, y) = \begin{cases} 2 & \text{if } r < 0.2, \\ 0.5 & \text{otherwise,} \end{cases} \quad (u, v)(0, x, y) = (0, 0), \quad p(0, x, y) = 1, \quad (25)$$

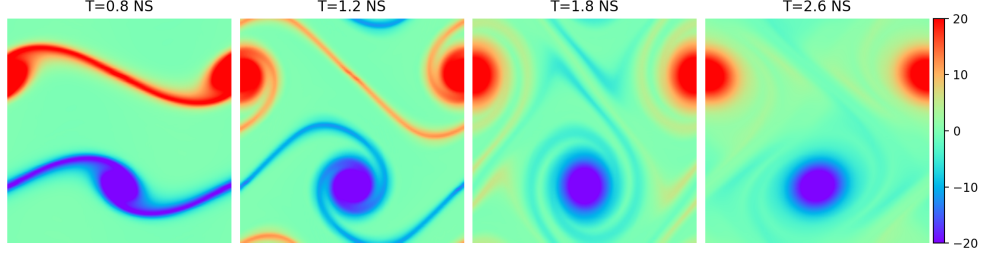


**Fig. 8** Double shear layer (Section 4.4): Vorticity contours with the Second order  $L^2$  AP scheme for the full Navier-Stokes equations setting  $\varepsilon = 10^{-3}$  and  $\mu = 2 \cdot 10^{-4}$  at times  $t = 0.8, 1.2, 1.8$  and  $2.6$  on a  $128 \times 128$  grid.

where  $r = \sqrt{x^2 + y^2}$ ,  $\varepsilon = 1$ ,  $\lambda = 10^{-2}$ ,  $\mu = 10^{-2}$  and  $t_{end} = 1$ . We set transmissive boundary conditions ( $\nabla W \cdot \nu = 0$ ) everywhere.

Figure 9, displays one-dimensional cuts of the temperature and heat flux along the  $x$  axis for  $y = 0$ . The simulations are run with the second order  $L^2$  and  $L^{2,stab}$  AP schemes until  $t = 1.0$ . Since we start with a velocity equal to  $(0, 0)$ , we have chosen a small time step until  $t = 0.01$  (related to the eigenvalues of the jacobian matrix associated to the inviscid flux i.e  $|U| \pm c$ ) and after  $t = 0.01$ , the usual restriction related only to the fluid velocity  $U$ . The solutions are in very good agreement with the exact reference solution.

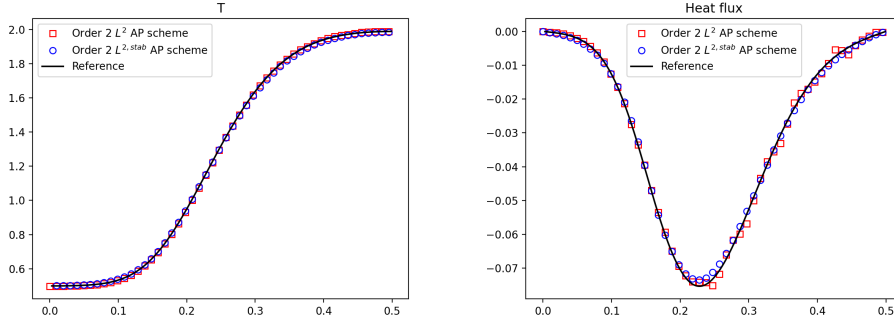


**Fig. 9** Heat conduction (Section 4.5): Temperature and heat flux at time  $t = 1.0$  with the second order  $L^2$  and  $L^{2,stab}$  AP schemes for  $101 \times 101$  points.

## 4.6 Lid-driven cavity flow: steady state incompressible solution

The following test case is well-known for the Navier-Stokes equations in the low Mach number regime. We consider a fluid in  $\Omega = [0, 1]^2$  with constant density and pressure and where the velocity is set to zero in all the domain except on the upper boundary where  $(u, v) = (1, 0)$ . The other three walls are stationary and we impose a no slip boundary condition  $(u, v) = (0, 0)$ . Then we expect the creation of a primary vortex at

the center of the cavity and secondary vortices on the bottom corners as the Reynolds number increases. The initial data are the following:

$$\rho(0, x, y) = 1, \quad u(0, x, y) = \begin{cases} 0 & \text{if } y < 1, \\ 1 & \text{if } y = 1, \end{cases} \quad v(0, x, y) = 0, \quad p(0, x, y) = 1, \quad (26)$$

with  $\varepsilon = 10^{-5}$ , no heat conduction  $\lambda = 0$  and  $\mu$  given by the Reynolds number  $R_e$ . The Reynolds number is defined by  $R_e = \rho_0 U_0 L / \mu$ , where  $\rho_0 = 1$ ,  $U_0 = 1$  and  $L = 1$  are respectively the characteristic density, velocity and length. Thus, we set  $\mu = 1/R_e$ . Moreover, in order to run the simulations we also impose a condition on the pressure:  $\nabla p \cdot \nu = 0$  on all the walls.

The simulation is run for different Reynolds numbers until a steady state is reached. For each simulation we show the final Mach number  $M = \sqrt{\varepsilon}|U|/c$  distribution, the  $u$  velocity contours along with the streamlines. We also compare the  $u$  and  $v$  velocity profiles along the lines  $y = 0$  and  $x = 0$  respectively with the reference solution given in [38] for the incompressible Navier-Stokes equations.

In Figure 10, we show the results for  $R_e = 100$  and time  $t = 20$  (top) and for  $R_e = 1000$  at time  $t = 30.0$  (bottom). On the left, we observe the Mach number varying in the range  $[0, 0.0027]$ . In the middle, we see as expected a primary vortex moving towards the cavity center and the formation of secondary vortices on the bottom corners as the Reynolds number increases. On the right row, the velocity profiles are in good agreement with the reference solution [38].

In Figure 11, we show the contour plots of pressure setting the Reynolds number to  $R_e = 1000$ . We compare the results given by the second order  $L^2$  and  $L^{2,stab}$  AP schemes. We can observe that some oscillations appear on the top corners for the ‘‘Second order  $L^2$  AP scheme’’ which vanish when adding the upwinding on the implicit part with the ‘‘Second order  $L^{2,stab}$  AP scheme’’.

## 5 Conclusion

Here, we proposed asymptotic preserving schemes for the Navier-Stokes equations allowing us to simulate viscous flows. The proposed discretization is based on a convective flux splitting ensuring the asymptotic stability and on an implicit treatment of the diffusive terms allowing us to be efficient also in highly viscous regimes. To obtain a simple linear scheme, we proposed a linearization of the pressure wave equation. For the new proposed scheme the asymptotic consistency is also proved on the semi-discretization. The scheme is extended to second order accuracy and a stabilization procedure based on an upwinding of the implicit convective solver is also proposed. Finally, we presented two dimensional numerical tests for a wide range of Mach numbers assessing the good behavior and asymptotic properties of our second order schemes both for the full Euler and the Navier-Stokes equations.

In future works, to further limit the non-physical oscillations, we aim to extend to the Navier-Stokes system the MOOD procedure proposed for the Euler equations in [26]. Furthermore, we have noticed that in some cases, the upwinding used in the implicit part of the convective flux to improve the stability can lead to excessive diffusion. This issue requires further investigation in order to appropriately choose the

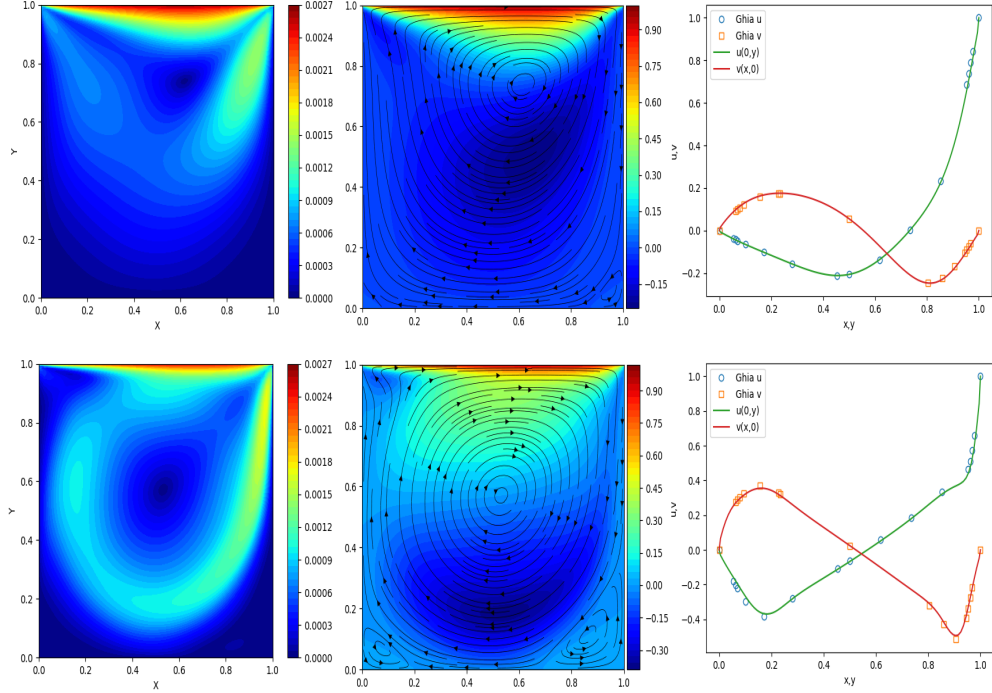


**Fig. 10** Lid driven cavity flow (Section 4.6): Results with the second order  $L^2$  AP scheme for  $Re = 100$  (top) and  $Re = 1000$  (bottom) on a  $100 \times 100$  grid. Mach number contours (left),  $u$  velocity contours with velocity streamlines (middle) and velocity profiles compared with the reference solution [38] (right).

implicit diffusion coefficient depending on the test-case. Finally, we believe that the performance of asymptotic preserving schemes for multiscale models can be enhanced by employing domain decomposition techniques. By dividing the computational domain into different regions, each with its own better suited numerical approach, we can achieve better performance.

## References

- [1] Barreau, G., Pechereau, F., Khiar, B., Lalande, P., Puigt, G., Vanharen, J., Alauzet, F.: Semi-implicit scheme for modelling the fluid dynamics part of a de-powered arc. (2023). Paper presented at the joint 10th EUCASS - 9th CEAS Conference, Lausanne, 9–13 July 2023
- [2] Barreau, G.: Application d’une méthode semi-implicite couplée avec des outils d’adaptation de maillage anisotropique pour modéliser des arcs continus (2024). PhD thesis, <https://theses.fr/2024ESAE0059>
- [3] Alazard, T.: Incompressible limit of the nonisentropic Euler equations with the solid wall boundary conditions. *Adv. Differential Equations* **10**(1), 19–44 (2005)

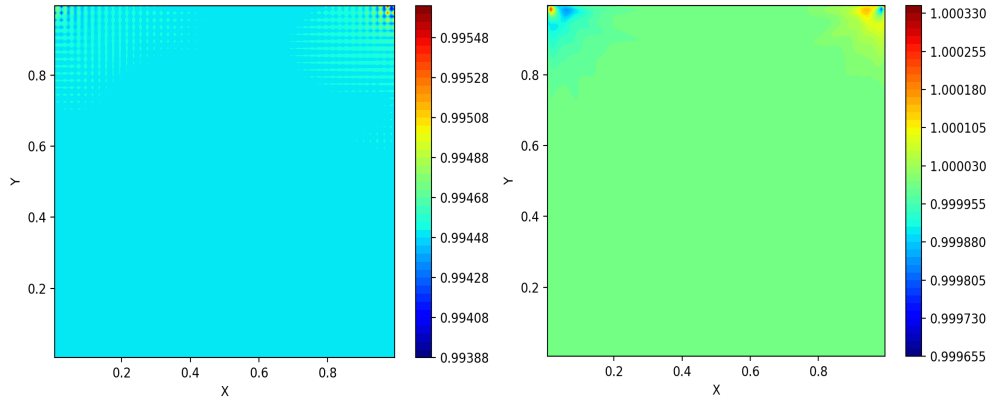


**Fig. 11** Lid driven cavity flow: Pressure contour plot for  $Re = 1000$  at  $t = 30.0$  given by the “Second order  $2 L^2$  AP scheme” (left) and by “Second order  $2 L^2,stab$  AP scheme” on a  $100 \times 100$  grid.

- [4] Klainerman, S., Majda, A.: Compressible and incompressible fluids. *Communications on Pure and Applied Mathematics* **35**(5), 629–651 (1982) <https://doi.org/10.1002/cpa.3160350503>
- [5] Schochet, S.: The compressible Euler equations in a bounded domain: Existence of solutions and the incompressible limit. *Communications in Mathematical Physics* **104**(1), 49–75 (1986) <https://doi.org/10.1007/BF01210792>
- [6] Metivier, G., Schochet, S.: The incompressible limit of the non-isentropic euler equations. *Archive for Rational Mechanics and Analysis* **158**, 61–90 (2001) <https://doi.org/10.1007/PL00004241>
- [7] Alazard, T.: Low mach number limit of the full navier-stokes equations. *Arch. Ration. Mech. Anal.* **180**, 1–73 (2006) <https://doi.org/10.1007/s00205-005-0393-2>
- [8] Danchin, R.: Zero mach number limit for compressible flows with periodic boundary conditions. *American Journal of Mathematics* **124**, 1153–1219 (2002)
- [9] Desjardins, B., Grenier, E., L., L.P., Masmoudi, N.: Incompressible limit for solutions of the isentropic navier-stokes equations with dirichlet boundary conditions. *Journal de Mathématiques Pures et Appliquées* **78**(5), 461–471 (1999) [https://doi.org/10.1016/S0021-7824\(99\)00032-X](https://doi.org/10.1016/S0021-7824(99)00032-X)
- [10] Lions, P.L., Masmoudi, N.: Incompressible limit for a viscous compressible fluid. *Journal de Mathématiques Pures et Appliquées* **77**(6), 585–627 (1998)
- [11] Toro, E.F.: *Riemann Solvers and Numerical Methods for Fluid Dynamics. A Practical Introduction*. Springer, Berlin (2009)
- [12] Guillard, H., Viozat, C.: On the behavior of upwind schemes in the low mach

- limit. *Comp. & Fluid* **28**, 63–86 (1999)
- [13] Guillard, H., Murrone, A.: On the behavior of upwind schemes in the low mach number limit : Ii. godunov type schemes. *Comp. & Fluids* **33**, 655–675 (2004)
- [14] Dellacherie, S.: Analysis of godunov type schemes applied to the compressible euler system at low mach number. *J. Comp. Phys.* **229**, 978–1016 (2010)
- [15] Chen, S.-S., Li, J.-P., Li, Z., Yuan, W., Gao, Z.-H.: Anti-dissipation pressure correction under low mach numbers for godunov- type schemes. *J. Comp. Phys.*, 111027 (2022)
- [16] Jung, V., Perrier, V.: Behavior of the discontinuous galerkin method for compressible flows at low mach number on triangles and tetrahedrons. *SIAM J. Sci. Comput.* **46**(1), 173–196 (1995)
- [17] Ascher, U.M., Spiteri, S.J., Ruuth, R.J.: Implicit-explicit Runge-Kutta methods for time-dependent partial differential equations. *Appl. Numer. Math. Special issue on time integration (Amsterdam, 1996)* **25**(2-3), 151–167 (1997)
- [18] Pareschi, L., Russo, G.: Implicit-explicit Runge-Kutta schemes for stiff systems of differential equations, in recent trends in numerical analysis. *Adv. Theory Comput. Math., Nova Sci. Publ., Huntington, NY* **3**, 269–288 (2001)
- [19] Allegrini, P., Vignal, M.-H.: Study of a new low-oscillating second-order all-mach number imex finite volume scheme for the full euler equations. *SIAM J. Sci. Comput.* **47**(1), 268–299 (2025) <https://doi.org/10.1137/23M1568703>
- [20] F., T.E., Vázquez-Cendón, M.E.: Flux splitting schemes for the euler equations. *Comput. Fluids* **70**, 1–12 (2012)
- [21] Dou, C., Jiang, S., Ou, Y.: Low mach number limit of full navier-stokes equations in a 3d bounded domain. *J. of Differential Equations* **258**(2), 379–398 (2015) <https://doi.org/10.1016/j.jde.2014.09.017>
- [22] Grenier, N., Vila, J.-P., Villedieu, P.: An accurate low-mach scheme for a compressible two-fluid model applied to free-surface flows. *J. Comp. Phys.* **252**, 1–19 (2013) <https://doi.org/10.1016/j.jcp.2013.06.008>
- [23] Bispen, G., Lukacova-Medvid’ova, M., Yelash, L.: Asymptotic preserving imex finite volume schemes for low mach number euler equations with gravitation. *J. Comp. Phys.* **335**, 222–248 (2017)
- [24] Dimarco, G., Loubère, R., Vignal, M.-H.: Study of a new asymptotic preserving scheme for the euler system in the low mach number limit. *SIAM J. Sci. Comput.* **39**(5), 2099–2128 (2017) <https://doi.org/10.1137/16M1069274>

- [25] Boscarino, S., Russo, G., Scandurra, L.: All mach number second order semi-implicit scheme for the euler equations of gas dynamics. *Journal of Scientific Computing* **77**, 850–884 (2017)
- [26] Dimarco, G., Loubère, R., Michel-Dansac, V., Vignal, M.-H.: Second-order implicit-explicit total variation diminishing schemes for the euler system in the low mach regime. *J. Comp. Phys.* **372**, 178–201 (2017)
- [27] Thomann, A., Zenk, M., Puppo, G., Klingenberg, C.: An all speed second order imex relaxation scheme for the euler equations. *Communications in Computational Physics* **28**(2), 591–620 (2020)
- [28] Tavelli, M., Dumbser, M.: A pressure-based semi-implicit space-time discontinuous galerkin method on staggered unstructured meshes for the solution of the compressible navier-stokes equations at all mach numbers. *J. Comp. Phys.* **341**, 341–376 (2016)
- [29] Boscheri, W., Dimarco, G., Loubère, R., Tavelli, M., Vignal, M.-H.: A second order all mach number imex finite volume solver for the three dimensional euler equations. *J. Comp. Phys.* **415**, 109486 (2020)
- [30] Boscheri, W., Pareschi, L.: High order pressure-based semi-implicit imex schemes for the 3d navier-stokes equations at all mach numbers. *J. Comp. Phys.* **434**, 110206 (2021) <https://doi.org/10.1016/j.jcp.2021.110206>
- [31] Leer, B.: Towards the ultimate conservative difference scheme v. a second-order sequel to godunov’s method. *J. Comp. Phys.* **135**, 229–248 (1997) <https://doi.org/10.1006/jcph.1997.5704>
- [32] Gottlieb, S., Shu, C.-W., Tadmor, E.: Strong stability-preserving high-order time discretization methods. *SIAM Review* **43**(1), 89–112 (2001) <https://doi.org/10.1137/S003614450036757X>
- [33] Schulz-Rinne, C.W., Collins, J.P., Glaz, H.M.: Numerical solution of the riemann problem for two-dimensional gas dynamics. *SIAM Journal on Scientific Computing* **14**(6), 1394–1414 (1993) <https://doi.org/10.1137/0914082>
- [34] Stokes, G.G.: On the effect of the internal friction of fluids on the motion of pendulums. *Transactions of the Cambridge Philosophical Society* **9**, 8–106 (1851)
- [35] Bell, J.B., Colella, P., Glaz, H.M.: A second-order projection method for the incompressible navier-stokes equations. *J. Comp. Phys.* **85**, 257–283 (1989)
- [36] Dumbser, M., Peshkov, I., Romenski, E., Zanotti, O.: High order ader schemes for a unified first order hyperbolic formulation of newtonian continuum mechanics coupled with electro-dynamics. *J. Comp. Phys.* **348**, 298–342 (2017) <https://doi.org/10.1016/j.jcp.2017.07.020>

- [37] Boscheri, W., Dimarco, G., Tavelli, M.: An efficient second order all mach finite volume solver for the compressible navier-stokes equations. *Computer Methods in Applied Mechanics and Engineering* **374**, 113602 (2021) <https://doi.org/10.1016/j.cma.2020.113602>
- [38] Ghia, U., Ghia, K.N., Shin, C.T.: High-re solutions for incompressible flow using the navier-stokes equations and a multigrid method. *J. Comp. Phys.* **48**, 387–411 (1982)